The heparan sulfate sulfotransferase 3-OST3A (HS3ST3A) is a novel tumor regulator and a prognostic marker in breast cancer

Mao, X.; Gauche, C.; Coughtrie, M. W. H.; Bui, C.; Gulberti, S.; Merhi-Soussi, F.

Published in:
Oncogene

DOI:
10.1038/onc.2016.44

Publication date:
2016

Document Version
Peer reviewed version

The heparan sulfate sulfotransferase 3-OST3A (HS3ST3A) is a novel tumor regulator and a prognostic marker in breast cancer

Xianqing Mao[1], Caroline Gauche[1], Michael W.H. Coughtrie[2,3], Catherine Bui[1], Sandrine Gulberti[1], Faten Merhi-Soussi[1], Nick Ramalanjaona[1], Isabelle Bertin-Jung[1], Alexandra Diot[2], Dominique Dumas[1,4], Nathalie De Freitas Caires[5], Alastair M. Thompson[6], Jean-Christophe Bourdon[2], Mohamed Ouzzine[1] and Sylvie Fournel-Gigleux[1]

Xianqing Mao and Caroline Gauche contributed equally to this work
Michael W.H. Coughtrie, Jean-Christophe Bourdon, Mohamed Ouzzine and Sylvie Fournel-Gigleux contributed equally to this work

Authors' Affiliations: [1]UMR 7365 CNRS-Université de Lorraine (IMoPA), MolCelTEG Team, Biopôle, Campus Biologie-Santé, Faculté de Médecine, Université de Lorraine, CS 50184, 54505 Vandoeuvre-les-Nancy, France; [2]Division of Cancer Research, Medical Research Institute, University of Dundee, Dundee, DD1 9SY, UK; [3]Faculty of Pharmaceutical Sciences, University of British Columbia, Vancouver, BC V6T 1Z3, Canada; [4]Cellular and Tissular Core Imaging Facility, PTIBC IBISA Nancy, FR3209 CNRS, 54500, Vandoeuvre-lès-Nancy, France; [5]INSERM, U1019E11, 59000, Lille, France ; [6]M. D. Anderson Cancer Center, University of Texas, 1400 Pressler Drive, Unit 1484, Houston, United States of America

Correspondance: Sylvie Fournel-Gigleux, UMR 7365 CNRS-Université de Lorraine (IMoPA), MolCelTEG Team, Biopôle, Campus Biologie-Santé, Faculté de Médecine, Université de Lorraine, CS 50184, 54505 Vandoeuvre-les-Nancy, France. Tel: + 33 3 83 68 54 08. E-mail: sylvie.fournel-gigleux@univ-lorraine.fr
Note: Current address for X. Mao: Laboratory of Cellular and Molecular Oncology, Luxembourg Institute of Health, Luxembourg
Running title: 3-OST3A: clinico-pathological impact in breast cancer

Heparan sulfate (HS) proteoglycan chains are key components of the breast tumor microenvironment that critically influence the behavior of cancer cells. It is established that abnormal synthesis and processing of HS play a prominent role in tumorigenesis albeit mechanisms remain mostly obscure. HS function is mainly controlled by sulfotransferases, and here we report a novel cellular and pathophysiological significance for the 3-*O*-sulfotransferase 3-OST3A (HS3ST3A), catalyzing the final maturation step of HS, in breast cancer. We show that 3-OST3A is epigenetically repressed in all breast cancer cell lines of a panel representative of distinct molecular subgroups, except in HER2-positive (HER2+) SKBR3 cells. Epigenetic mechanisms involved both DNA methylation and histone modifications, producing different repressive chromatin environments depending on the cell molecular signature. Gain and loss of function experiments by cDNA and siRNA transfection revealed profound effects of 3-OST3A expression on cell behavior including apoptosis, proliferation, response to trastuzumab *in vitro* and tumor growth in xenografted mice. 3-OST3A exerted dual activities acting as tumor-suppressor in lumA-MCF-7 and triple negative-MDA-MB-231 cells, or as an oncogenic factor in HER2+-SKBR3 cells. Mechanistically, fluorescence-resonance energy transfer (FRET)-fluorescence-lifetime imaging microscopy (FLIM) experiments indicated that the effects of 3-OST3A in MCF-7 cells were mediated by altered interactions between HS and fibroblast growth factor-7 (FGF-7). Further, this interplay between HS and FGF-7 modulated downstream ERK, AKT and p38 cascades, suggesting that altering 3-*O*-sulfation affects FGFR2IIIb-mediated signaling. Corroborating our cellular data, a clinical study conducted in a cohort of breast cancer patients uncovered that, in HER2+ patients, high level expression of 3-OST3A in tumors was associated with reduced relapse-free survival. Our findings define 3-OST3A as a novel regulator of breast cancer pathogenicity, displaying tumor-suppressive or oncogenic activities in a cell- and tumor-dependent context, and demonstrate the clinical value of the HS-*O*-sulfotransferase 3-OST3A as a prognostic marker in HER2+ patients.

Key words: Heparan sulfate synthesis, sulfotransferase, epigenetic, breast cancer, biomarker

INTRODUCTION

Heparan sulfate proteoglycans (HSPG) are integral components of extracellular matrices and cell plasma membranes. They are key determinants of the relationships cells have with each other and with their microenvironment, and their role in cancer biology is increasingly recognized.[1] HS glycosaminoglycan chains of cell surface PG, strategically located at the cell-matrix interface, act as co-receptors for numerous signal transduction pathways. HS are composed of uronic acid and *N*-acetylglucosamine repeating disaccharide units covalently attached to the core protein of PG through a tetrasaccharide linkage region.[2] During biosynthesis, HS are subjected to marked structural modifications - mainly epimerization, *N*-deacetylation, *N*- and *O*-sulfation, catalyzed by numerous enzymes, including HS-*O*-sulfotransferases.[3,4] The range of biological functions of HS ultimately depends on the fine structure of their polysaccharide chain. The 3-*O*-sulfotransferases (3-OST) form the largest multigene family of HS modifying enzymes with seven different isoforms, catalyzing *O*-sulfation at position 3 of glucosamine (GlcN) residues to produce at least two functionally distinct 3-*O*-sulfated motifs. Importantly, this relatively rare modification completes the fine-tuning of HSPG and is responsible for highly specific HS activities.[5] The best characterized is the anticoagulant property of the 3-*O*-sulfated anti-thrombin binding motif, primarily generated by the 3-OST1 isoform. Although it is mostly documented that 3-OST3A generates receptors for *Herpes simplex* virus type-1 (HSV-1) entry[6], other likely biological functions, such as regulation of growth factors and their tyrosine kinase receptors signaling remain to be explored.

HSPG are critical effectors of several hallmarks of cancer biology.[7] In tumor cells, genes involved in the biosynthesis of HSPG are frequently dysregulated. The upregulation of cell-surface HSPG glypican-1 and syndecan-1 has been described in malignant breast cancer tissue[8], whilst depletion of the extracellular sulfatase Sulf-1 was reported.[9] Disruption of HS biosynthetic enzymes results in changes in HS fine structure that critically affect cell-matrix interactions, cell signaling and tumor cell behavior, including proliferation, adhesion, migration and apoptosis through interplay of complex mechanisms.[10]

Recent studies highlight an aberrant modulation of *3-OST* gene expression through epigenetic mechanisms in various tumors including breast, lung, brain, pancreatic, skin and colorectal cancers, suggesting an important role in these pathological conditions.[11,12] However, these reports reveal either anti-oncogenic or tumor-promoting effects, and the mechanisms and consequences of *3-OST* dysregulation in the cancer process are thus not well understood.[13,14] We recently showed that epigenetic repression of *3-OST* genes in chondrosarcoma cells leads to altered HSPG sulfation, and demonstrated tumor-suppressive properties of 3-*O*-sulfation in chondrosarcoma cells.[15]

Identification of the molecular mechanisms underlying the role of HS-modifying enzymes in breast cancer may open new windows for the design of personalized therapies to overcome drug failure and for the discovery of new biomarkers. Here, we demonstrate a critical role of 3-OST3A in specific breast cancer subtypes. We showed epigenetic repression of 3-OST3A in several breast cancer cell lines, and demonstrated its impact on cancer cell behavior by

gain and loss of function approaches. Importantly, we examined the influence of 3-OST3A expression on clinical outcome in a cohort of breast cancer patients. Our study identifies the HS-sulfotransferase 3-OST3A as a novel tumor regulator exerting either tumor-suppressive or oncogenic properties in a cell-dependent context, and demonstrates its potential clinical value as a prognostic marker in HER2+ breast cancer patients enabling stratification of patients for treatment.

RESULTS

3-OST3A is differentially repressed in breast cancer cell lines *via* epigenetic mechanisms

Prompted by studies from us and others pointing to an epigenetic control of *3-OST* genes[11,15], we determined whether *3-OST3A* was regulated epigenetically in breast cancer cells. 3-OST3A expression analysis in a panel of cell lines representative of distinct molecular subgroups of breast cancer (luminal-A [lumA]: ER+ PR+ HER2-; luminal-B [lumB]: ER+ PR+/- HER2+/-; HER2+: ER- PR- HER2+; triple-negative [TN]: ER- PR- HER2-[16], Table S1) revealed very low mRNA level in BT-474, T-47D and MDA-derived cells, and reduced expression in lumA-MCF-7 cells compared to the non-tumorigenic epithelial-derived MCF-10A cells (Figure 1A). The highest expression level was for HER2+-SKBR3 cells.

DNA methylation analysis of the *3-OST3A* promoter CpG island (Figure S1A) showed strong hypermethylation in T-47D and MDA-derived cells, while in MCF-7 cells, hypermethylation only occurred downstream from the TSS (Figure 1B). In contrast, *3-OST3A* was not subject to DNA methylation in SKBR3 and MCF-10A cells (Figure 1B and S1B). We established further a link between *3-OST3A* hypermethylation and gene expression by treating the MCF-7 and MDA-MB-231 cells with 5-aza-2'-deoxycytidine (Aza, DNAmethyltransferase (DNMT) inhibitor) and trichostatin A (TSA, histone deacetylase (HDAC) inhibitor). In MCF-7 cells, Aza and TSA alone markedly increased 3-OST3A mRNA level (Figure 1C), while no additive effect was observed upon combined treatment. Conversely in MDA-MB-231 cells, neither Aza nor TSA independently produced a significant effect, whereas combined treatment increased expression, suggestive of a co-operative action between histone deacetylation and DNA methylation (Figure 1C).

To provide insight into the differential regulation of 3-OST3A in MCF-7 and MDA-MB-231 cells, representative of the lumA and TN subtype, respectively, we analyzed several epigenetic marks at the *3-OST3A* promoter. We first evaluated the abundance of DNMT3A and 3B isoforms, and of DNMT1 involved in *de novo* and maintenance of DNA methylation, respectively (Figure 2A). We next examined several Polycomb group (PcG) proteins that form large complexes generally associated with CpG island promoters and cause closure of local chromatin mainly by affecting histone modifications[17]. We investigated here enhancer of zeste homolog 2 (EZH2) that trimethylates Lys27 of histone 3 (H3K27me3) and is associated with the suppressor of zeste 12 (SUZ12) protein to form part of Polycomb repressive complex PRC2. To further investigate the crosstalk between DNA methylation and

histone modifications, the methyl-CpG-binding protein 2 (MeCP2) that recruits histone deacetylases (HDACs) to the methylated regions[18] as well as Sin3A that functions as a corepressor complex with HDACs and MeCP2[19] were investigated. In MCF-7 cells, enrichment in DNMT3B (Figure 2B) was associated with a strong increase in the repressive H3K27me3, but not in the other repressive trimethylated Lys9 of histone 3 (H3K9me3, Figure 2C) histone mark. As expected, a decrease in the active mark trimethylated Lys4 of histone 3 (H3K4me3) was observed compared to MCF-10A (Figure 2C).
In MDA-MB-231, a strong increase in abundance of DNMT1 and DNMT3A was associated with the presence of repressive H3K9me3 and H3K27me3 and with the depletion of H3K4me3 (Figure 2B and 2C). As expected, in MCF-10A cells H3K4me3 was abundant and H3K9me3 and H3K27me3 absent (Figure 2C). Interestingly, although 3-OST3A regulation in SKBR3 cells does not involve DNA methylation, ChIP analysis suggested that it could involve histone modifications (data not shown). The histone H3K27 methyltransferase EZH2 was abundantly associated with the *3-OST3A* gene in MDA-MB-231 whereas it was less recruited in MCF-7 cells, while SUZ12 was present at low levels (Figure 2D). These data suggest that proteins of the PRC2 complex mediate *3-OST3A* gene repression in combination with DNMT3B in MCF-7 cells, and with DNMT1 and 3A in MDA-MB-231. Investigation of the crosstalk between DNA methylation and histone modifications showed that in MCF-7 cells the recruitment of HDAC1 did not require MeCP2 (Figure 2E), in agreement with the observation that Aza and TSA derepressed the promoter independently. Conversely in MDA-MB-231 cells, MeCP2, HDAC1 and Sin3A were enriched at the *3-OST3A* locus (Figure 2E). Such repressive environment might explain why treatment with both deacetylation and methylation inhibitors is required to reactivate *3-OST3A* expression in the latter cells. The distinct repressive complexes in the two cell lines are schematically depicted in Figure 2F.

3-OST3A exerts tumor-suppressive or pro-oncogenic effects depending on tumor cell phenotype and influences response to trastuzumab

Having demonstrated different expression level and epigenetic behavior in lumA-MCF-7, TN-MDA-MB-231, and HER2+-SKBR3 cells, we next interrogated the functional impact of 3-OST3A expression in these cell lines by gain and loss of function experiments. Overexpression moderately reduced cell growth rate in MCF-7 cells and completely inhibited cell proliferation in MDA-MB-231 cells (Figure 3A). Importantly, in SKBR3 cells, 3-OST3A expression produced the opposite effect, enhancing proliferation, whereas its knockdown by siRNA transfection consistently reduced cell growth (Figure 3A). These data emphasize the cell-context dependent outcome of HS 3-*O*-sulfation upon 3-OST3A overexpression or silencing, that we showed by performing immunofluorescence staining experiments using specific HS4C3 antibodies[20] (data not shown). A cornerstone of HER2 therapeutic strategies involves the use of a humanized monoclonal anti-HER2 antibody (trastuzumab) leading us to analyze the influence of 3-OST3A expression on HER2+-SKBR3 drug response. Significantly, trastuzumab exerted a stronger antiproliferative effect in 3-OST3A-expressing than in vector-transfected cells, whereas its influence was abrogated following 3-OST3A

siRNA knockdown (Figure 3B), indicating that 3-OST3A not only acts as a tumor regulator but also modulates anticancer drug sensitivity.

Analysis of apoptosis using Annexin V staining showed that 3-OST3A expression was pro-apoptotic in MCF-7 cells (Figure 4A), but not in MDA-MB-231 and SKBR3 cells (Figure S2). Further investigation of the cell survival mechanisms in MCF-7 cells showed enhanced expression of the pro-apoptotic protein Bax and decreased expression of the anti-apoptotic Bcl-2 (Figure 4B). 3-OST3A also activated caspase-mediated apoptosis, producing an increase in cleaved caspase 9 and in the proteolytic cleavage of poly(ADP-ribose)polymerase (PARP) (Figure 4B). This was accompanied by DNA fragmentation, as shown by a TUNEL assay (Figure 4C). These lines of evidence indicating that 3-OST3A expression results in reduced cell growth and promotes cell survival in MCF-7 cells prompted us to investigate its effect in xenografted mice.

SCID mice were transplanted with genetically engineered MCF-7-3-OST3A cell lines in two separate experiments (Figure 4D). A clear trend towards reduced tumor size was observed in mice implanted with MCF-7-3-OST3A-A cells compared with empty vector-transfected cells, reaching significance at 6 and 12 weeks (Figure 4E, and S3A). Moreover, MCF-7-3-OST3A-B cells exhibited retarded tumor progression from 8 to 18 weeks following implantation (Figure 4F and S3B). Together, these *in vivo* experiments provide strong supporting evidence for the 3-OST3A pro-apoptotic and antiproliferative properties observed *in vitro*, indicating that 3-OST3A acts as a tumor-suppressor in a model of lumA breast tumors.

3-OST3A affects FGF-7-HS interactions and regulates FGF-7 signaling

HSPGs influence the tumor process by regulating the activity of a variety of signaling molecules, primarily FGFs.[21] FGF-7 (keratinocyte growth factor) acting on epithelial cells[22] is a potent mitogen for mammary glands[23,24], and induces proliferation and motility in breast cancer cells.[25] This led us to explore the influence of 3-OST3A expression on FGF-7-HS interactions and signaling. FGF-7 binding was analyzed by confocal microscopy, flow cytometry and, to directly assess FGF-7 and HS interactions, by FRET-FLIM assays in MCF-7 cells compared to MCF-10A cells. siRNA transfected MCF-10A cells displayed a strong pericellular immunofluorescent staining pattern, consistent with enhanced FGF-7 binding, whereas FGF-7 staining was reduced in MCF-7 upon 3-OST3A expression (Figure 5A and 5B). Quantitative flow cytometry clearly confirmed an increase in fluorescence signal associated with FGF-7 binding in siRNA transfected MCF-10A, and a decrease in 3-OST3A transfected MCF-7 cells (Figure 5C).

In a FRET assay (Figure S4), a clear increase in emission intensity of HS-AlexaFluor 555 was observed in empty vector transfected MCF-7 cells compared to those transfected with 3-OST3A (Figure S4A). Lambda scan showed a significant FRET from FGF-7-AlexaFluor 488 to HS-AlexaFluor 555 in cells that did not express 3-OST3A-HA (Figure S4B). FLIM analysis confirmed a greater distribution in favor of the FRET positive cell population (in green) in control cells, compared to 3-OST3A transfected cells (Figure 5D). The average

lifetime of AlexaFluor 488 was unchanged in cells expressing 3-OST3A-HA, but reduced in control and 3-OST3A-HA-negative cells (Figure 5E, Table 1). These data indicate that binding of FGF-7 is HS-dependent, and that it is impaired upon 3-OST3A overexpression in MCF-7 cells, highlighting the potential impact of 3-*O*-sulfation on FGF-7-HS interactions.

We next examined whether impaired FGF-7-HS interactions mediated by 3-OST3A would affect FGF-7 downstream signaling pathways. FGF-7 activates the Ras-MAP kinase and PI3K-AKT cascades following binding to its receptor FGFR2IIIb, a splice variant of FGFR2 expressed in breast carcinoma cell lines.[26,27] Indeed, phosphorylation of AKT was reduced upon FGF-7 treatment at low dose in 3-OST3A-transfected MCF-7 cells (Figure 5F). Furthermore, ERK phosphorylation was strongly inhibited upon 3-OST3A transfection from 0.5 to 1 ng/mL (Figure 5G), whereas phosphorylation of p38 was increased in response to FGF-7 treatment (Figure 5H). In empty vector transfected MCF-7 cells, a slight increase in ERK phosphorylation was observed at the highest FGF-7 concentration and exposure time (Figure S5A) whereas no variations in AKT and p38 phosphorylation occurred (Figure S5B and C). Our results suggest that inactivation of the FGF-7-induced ERK signaling pathway is involved in the antiproliferative effect of 3-OST3A in lumA-MCF-7 cells, and that inhibition of FGF-7-AKT, together with activation of FGF-7-p38 signaling, contributes to its pro-apoptotic effect (as represented Figure S6).

3-OST3A is a prognostic marker in breast cancer patients

To assess the clinical relevance of our experimental data, we analyzed 3-OST3A expression in a cohort of primary breast tumors.[28] The cohort was segregated into 4 subtypes *i.e.* lumA, lumB, HER2+ and TN according to the pathological markers recommended by the St Gallen breast cancer consensus guidelines[16] (Table S2). Consistent with other clinical studies, TN and HER2+ breast cancers were the most aggressive breast cancers (Figure S8A). All tumors expressed 3-OST3A (Figure 6A) and Kruskal-Wallis analysis indicated that the level of 3-OST3A expression was associated with the breast cancer subtype ($P<0.017$). Importantly, 3-OST3A expression was significantly lower in lumA-tumors compared to other breast cancer subtypes (Mann-Whitney, $P<0.042$). This observation suggested that a low expression of 3-OST3A contributes to the cancer process in lumA tumors, as corroborated by the tumor-suppressive effect mediated by 3-OST3A overexpression in MCF-7 cells (shown Figure 3A and 4A). On the other hand, 3-OST3A expression was significantly higher in HER2+ tumors (Mann-Whitney, $P<0.008$), suggesting that in this subtype, elevated 3-OST3A would favor breast cancer formation and progression, in accordance with its oncogenic properties in SKBR3 cells (shown Figure 3A).

We next investigated the relationship between 3-OST3A expression and HER2+ patient outcome. The optimal cut-off for HER2+ breast tumours was determined by ROC curves[29,30] (Figure S7). Importantly, we showed using univariate analysis that 3-OST3A expression was significantly associated with cancer progression (CP) (Fisher exact *t* test; $P\leq0.004$) and death ($P\leq0.046$) in HER2+ breast tumors (Table S3). This was confirmed by Kaplan-Meier log-rank analyses (CP, $\chi^2 = 7.221$, 1 df, $P\leq0.007$; death, $\chi^2 = 3.686$, 1 df, $P\leq0.055$, Figure 6B).

In addition to 3-OST3A expression (3ost), tumor size (S) and lymph node metastasis (LN, absence or presence) were independently associated with CP in HER2+ breast cancers (Figure S8B and C, Table S4-6). We then formed a binary variable (3ost, S, LN) that was positive only when the HER2+ patients had a 3-OST3A positive tumor of a diameter larger than 20 mm and at least one lymph node metastasis (Figure 6C). Multivariate Cox's regression analysis determined the interdependence degree between these three parameters and confirmed that the combined variable (3ost, S, LN) stood out as an independent significant predictor of cancer recurrence and death (Table 2). This positive variable (3ost, S, LN) enhanced 27-fold the risk of recurrence (Hazard ratio (HR), 27.3; 95% Confidence Interval (CI), 3.6 to 207.7). The Omnibus test indicated that the number of HER2+ breast tumors is sufficient to support this conclusion (Table 2). The Cox's Regression analysis was further confirmed by Kaplan-Meier log-rank analyses (CP: $\chi^2 = 23.233$, 1 df, $P<2.10^{-6}$, death: $\chi^2 = 14.354$, 1 df, $P<2.10^{-4}$, Figure 6C) indicating that the combined variable (3ost, S, LN) separated two subtypes of HER2+ breast cancer patients with opposite clinical outcome.

The HER2+ breast cancer patients positive for (3ost, S, LN) represented 43% of total HER2+ patients and among these patients, 71% (15/21) suffered from recurrence (Figure 6C) compared to 44% (16/36) when considering 3-OST3A expression only (Figure 6B), thus providing a discriminating biomarker for clinicians. Considering the combined variable allowed the identification of 93% (15/16) of patients in whom cancer recurred or who died, while the HER2+ patients negative for (3ost, S, LN) had no recurrence over 15 years. Our results suggest that the current treatment of HER2+ patients is efficient in 96% (27/28) of the (3ost, S, LN) negative patients, while the HER2+ breast cancer patients positive for (3ost, S, LN) would benefit from additional or alternative treatment such as trastuzumab.

DISCUSSION

This study reports for the first time the molecular, functional and clinical role of the HS-sulfotransferase 3-OST3A, a key enzyme controlling the tumor microenvironment, in breast cancer. A main result of our work is the unequivocal demonstration that 3-OST3A can display either oncogenic or tumor-suppressive effects depending on the cell and tumor phenotype. This detailed analysis clarifies conflicting literature that reports contrasting effects of 3-OSTs expression on tumorigenesis in different types of cancer and cell models.[13,14] Importantly, the clinical study performed here shows that 3-OST3A is differentially expressed in distinct subtypes of tumors, corroborating our *in vitro* data, and establishes the prognostic value of 3-OST3A as a novel marker in HER2+ breast cancer patients.

Previous reports including ours have documented the epigenetic repression of several *3-OST* genes in tumor cells.[11,15,31] Our study shows that 3-OST3A was repressed and subjected to hypermethylation in all breast cancer cell lines tested except in HER2+-SKBR3 cells in which, consistently, it was expressed at relatively high level. Further analysis of the chromatin interactors at the *3-OST3A* promoter showed that the epigenetic regulation not only depends upon DNA methylation, but also on repressive histone marks, and involves the

recruitment of PcG proteins. We describe here for the first time a fine interplay between DNA methylation, histone modifications and epigenetic regulators of the PRC2 complex controlling 3-OST3A expression in a cell-context dependent manner. In lumA-MCF-7 cells, DNMT3B and the EZH2 subunit of the PRC2 complex involved in writing the repressive H3K27me3 mark form a chromatin environment that moderately repressed transcriptional activity. In MDA-MB-231 cells, we propose a scenario at the *3-OST3A* promoter in which the methylated DNA reader MeCP2 is associated with a deacetylase complex formed by Sin3A, HDAC1 and possibly H3K9 methyltransferases.[18] Altogether the chromatin interactors DNMT1, 3A, PcG proteins and the histone marks H3K27me3 and H3K9me3 produce gene silencing in these cells. Our demonstration of the HS-sulfotransferase *3-OST3A* gene methylation and histone modification is in line with previous findings indicating that epigenetic dysregulation is an important feature of breast cancer pathobiology and that it depends upon the tumor signature.[32] Our results validate the potential value of epigenetic therapies targeting *3-OST3A* together with other silenced critical genes such as those coding for the Ras interacting protein RASSF1A[33], the estrogen receptor α (ERα)[34] and the retinoic acid receptor RARα[35] in TN breast cancers. Altogether, our findings support the attractive idea that the HS-modifying 3-OST3A sulfotransferase enzyme participates ino the matrix-cell dialog through epigenetic mechanisms.

FGFs, a significant group of HS ligands, use HSPG as co-receptors to bind specific tyrosine kinase receptors promoting signal transduction, and FGF signaling is deregulated in many cancer types.[36] We thus hypothesized that *3-OST3A* epigenetic regulation may alter breast cancer cell phenotype through modulation of FGF-dependent intracellular signaling. FGF-7 secreted by stromal mesenchymal cells acts on epithelial cells, where it associates with the FGFR2IIIb receptor. Alteration of the FGF-7-FGFR2IIIb signaling axis contributes to the oncogenic process by activating intracellular kinase cascades including ERK-dependent proliferation and AKT-mediated cell survival in breast cancer cells[37], and anti-FGFR2IIIb antibodies offer a new therapeutic option.[38] Since FGF-7 is one of the most structurally specific FGFs with respect to its requirement for a 3-*O*-sulfated motif to coordinate ligand-receptor complex assembly[39,40], we investigated whether 3-OST3A expression may regulate its signaling pathway to trigger the tumor-suppressive effect observed in the lumA-MCF-7 cells. Supporting this assumption, our data show that reinstating 3-OST3A expression in these cells: *i*) impaired interactions between FGF-7 and HS chains, *ii*) inhibited proliferative signals *via* ERK dephosphorylation, and *iii*) boosted apoptotic signals *via* AKT dephosphorylation and p38 phosphorylation. Our observations are of particular interest since FGF-7 plays a critical role both in mammary gland development and breast cancer onset and progression.[41] Since 3-*O*-sulfation is an important modification of HS for HS-FGF-7-FGFR2IIIb complex formation[42], our data support the idea that this modification might contribute to the anti-oncogenic properties of 3-OST3A in lumA cells. However, it is of note that the mechanisms underlying impaired FGF-7 binding in MCF-7 cells upon 3-OST3A expression is not fully understood. We ruled out the possibility that 3-OST3A would reduce FGFR2IIIb expression (data not shown). On the other hand, according

to several reports[43], it is hypothesized that 3-*O*-sulfated HS binding may precede and prevent FGF-7 interactions with its FGFR2IIIb receptor. Another possibility is that altered activation of fibroblast growth factor receptor substrate 2 (FRS2α) would trigger internalization and degradation of FGFR2IIIb thus contributing to attenuate FGF-7 binding and signaling seen in our experiments upon 3-OST3A expression. These options are currently under investigation in our laboratory.

Since the effects triggered by 3-OST3A expression in breast cancer cell lines depended on their molecular signature, a major aim of the present study was to evaluate the clinico-pathological impact of 3-OST3A expression in breast cancer. We provided insight into this key issue by conducting a clinical study in a cohort of breast cancer patients followed over a 15-year period. The low expression detected in lumA tumors suggests that 3-OST3A might inhibit cancer formation and progression and is consistent with a tumor-suppressive effect in this subtype of malignancies. This assumption is supported by our experimental data showing a pro-apoptotic and anti-proliferative effect triggered by 3-OST3A expression in MCF-7 cells, associated with tumor growth retardation in xenografted mice.

A key finding is that, in HER2+ subtype breast cancer patients, high 3-OST3A expression is associated with reduced survival. The SKBR3 cell model harboring this molecular signature allowed us to explore the mechanisms underlying our clinical observations. Consistently, we showed that 3-OST3A overexpression in SKBR3 cells promotes proliferation, whereas its silencing results in the reverse effect. Furthermore, 3-OST3A expression enhanced the antiproliferative effect of trastuzumab whereas knocking-down expression arrested it. This result has two important outcomes. First, it suggests that 3-OST3A-mediated HS modification alters the HER2 receptor-mediated signaling pathway, an assumption that is currently under investigation. Second, it reveals a novel and potentially clinically important effect of 3-OST3A on sensitivity to the therapeutic anti-HER2 antibody trastuzumab. Identifying the HER2+ breast cancer patients who might benefit from extended adjuvant therapy represents a long-standing conundrum. In our cohort, about 40% of HER2+ breast cancer patients given chemotherapy (5-fluorouracil, epirubicin (doxorubicin) and campthothecin) suffered from cancer progression, a poor outcome highlighting a currently unmet clinical need. This phenomenon, strongly supported by the data presented here, could therefore facilitate the stratification of two populations of HER2+ breast cancer patients; one 3-OST3A positive population with at least one lymph node metastasis and a tumor diameter greater than 21 mm who are much more likely (71% chance) to suffer from cancer recurrence and death, and thus would clearly benefit from alternative therapy such as trastuzumab, while the 3-OST3A negative population has a much better prognosis with lack of recurrence over 15 years.

In conclusion, we show that the sulfotransferase 3-OST3A, involved in the final step of HS processing, is a key regulator of tumor cell behavior and anticancer drug response, and that its oncogenic or tumor-suppressive effects are cell- and tumor-signature dependent. The finding that 3-OST3A expression correlates with cancer progression in HER2+ patients highlights its clinical significance for guiding therapeutic options in breast cancer treatment.

MATERIALS AND METHODS

Cell culture, drug treatment and transfection

Human breast cancer cell lines SKBR3, BT-474, T-47D, MDA-MB-231, MDA-MB-453 and MDA-MB-468 representative of distinct molecular subgroups (Table S1) and the immortalized breast epithelial cell line MCF-10A were from the American Type Culture Collection (ATCC). The MCF-7 cell line was from the European Collection of Cell Cultures (ECACC). Detailed culture conditions and treatment by Aza and TSA are described in Supplementary Materials. Cell lines were transiently or stably transfected with pcDNA3.1(+)-3-OST3A-hemagglutinin (HA) or the pcDNA3.1(+) plasmid[15,44] and 3-OST3A expression was analyzed by immunoblotting using anti-HA antibodies (Table S7). 3-OST3A siRNAs (Eurogentec, Table S8) and a negative control (Qiagen) were transfected as in Supplementary Materials. siRNA efficacy was verified by RT-qPCR and protein analysis.

RT-qPCR analysis

Total RNA was extracted and purified using the RNeasy Mini kit (Qiagen) for cultured cells and the QIAzol Lysis reagent (Qiagen) for tumor samples. mRNA level was quantified by the $2\text{-}\Delta\Delta C_t$ method using primers listed in Table S9.

CpG island identification, methylation analysis and chromatin immunoprecipitation (ChIP) assay

Genomic DNA was purified using the GenomicPrepDNA isolation kit (GE Healthcare). The presence of a canonical CpG island in the proximal promoter region (5') and first exon (3') of *3-OST3A* gene was determined using MethPrimer software. The methylation status of two regions was analyzed by bisulfite sequencing[15] using sense and antisense primers for nested-PCR (Table S10). PCR products subcloned into TOPO-TA® vector (Invitrogen) were sequenced in at least three clones. ChIP assay was performed using the Low Cell# ChIP kit (Diagenode) using antibodies and PCR primers described in Tables S11 and S12, respectively.

Protein analysis

Immunoblot following SDS-PAGE analysis of cell lysate proteins was performed using primary and secondary antibodies listed in Table S7.

FGF-7 cell-surface binding assays

Cells cultured in Lab-Tek chambers (Thermo-Scientific) or 6-well plates were serum-starved and incubated with recombinant human FGF-7 (0.5 ng/mL) for 30 min. Cells were immunostained for FGF-7 and HS expression using antibodies (Table S7) prior to confocal laser scanning microscopy. Alternatively, following immunostaining, cells were fixed in 4% (w/v) *para*formaldehyde prior to flow cytometry (Gallios, Beckman Coulter).

FLIM-based FRET Assay

For the image series and spectra measurements, a Leica TCS SP5-X-AOBS microscope equipped with an acousto-optical beamsplitter and WLL lasers was used with a ×40/0.8 water immersion objective. Temporal histogram depicting the AlexaFluor 488 fluorescence lifetime was obtained by a biexponential fit of the fluorescence decay. The decay analysis by time-correlated single photon counting was performed using the SPCImage software (Becker&Hickl).

Cell apoptosis assays

After transient transfection with empty vector or with 3-OST3A-HA cDNA and with siRNA control or siRNA 3-OST3A in the case of SKBR3 cells for 48 h, cells were stained with AlexaFluor 488-conjugated annexin V and propidium iodide (PI) dyes (Invitrogen). The externalization of phosphatidylserine (PS) and the permeability to PI were evaluated by flow cytometry. A TUNEL test was also performed on MCF-7 cells transfected with empty vector or with 3-OST3A-HA cDNA.

Cell proliferation assay

Twenty four hours after transfection with 3-OST3A-HA cDNA, and with siRNA 3-OST3A and corresponding controls, MCF-7, MDA-MB-231 and SKBR3 cells were harvested each day during a 4-day period and cell proliferation was evaluated by measuring DNA content. Cell proliferation was also assessed 2 days following transient transfection in SKBR3 cells treated with 0, 20 and 40 µg/mL trastuzumab kindly provided by Dr. Catherine Vallance (Institut de Cancérologie de Lorraine, Vandoeuvre-les-Nancy, France).

In vivo mouse xenograft tumor model

Experiments were performed in 6-week-old female severe combined immunodeficient (SCID) mice. MCF-7 cells stably expressing 3-OST3A-HA or transfected with pcDNA empty vector were subcutaneously implanted into the animals. 5×10^6 cells were injected into each mouse (four mice/group for each independent experiment). The tumor growth was assessed weekly using a Vernier caliper. The experiment was conducted twice using two different engineered MCF-7 cell lines denominated 3-OST3A-A and -B, and pcDNA-A and -B, respectively.

Breast tumor sample analyses

3-OST3A mRNA expression was analyzed in a cohort of 117 primary breast tumors collected at Ninewells Hospital, Dundee, UK from Caucasian women with no previous treatment or operation (Tayside Tissue Bank (TTB), Dundee, UK). Informed consent was obtained from all patients and ethical approval was received from TTB (REC Reference: 07/S1402/90) under delegated authority from the Local Research Ethics Committee. Breast cancer overall survival (overall survival) and breast cancer-specific disease free survival

(disease free survival or cancer recurrence) were considered. Non-breast cancer deaths (women died from other causes than breast cancer) were censored. The characterization of classical molecular markers was conducted as previously described.[45] Histological tumor grade was according to Bloom et al.[46], ER status according to Quickscore method[47] and HER2+ scoring according to Purdie et al.[48]

Statistical analysis

Data were analyzed using Prism software (GraphPad, San Diego, CA) and are expressed as mean±SEM of two replicates in at least three independent experiments. One-way ANOVA and Tukey's post-hoc test were used for analysis of data from cell proliferation and FLIM assays. Two-way ANOVA and Bonferroni post-hoc tests were used to calculate differences in tumor growth. Paired Student's *t* test was used to calculate *P* values for all other experiments. *P* value <0.05 was considered significant.

Statistical univariate analyses (Kaplan-Meier and Log Rank test) of clinical data were performed using SPSS software (SPSS, version 21.0) followed by multivariate analyses of Cox's proportional hazards regression model (CR) with associated Hazard Ratios (HR) utilizing the backwards step-wise elimination method.

Experimental Procedures are detailed in the Supplementary Materials and Methods section.

Disclosure of Potential Conflicts of Interest

No conflicts of interest were declared

Financial support

This work was supported by Agence Nationale de la Recherche (ANR-GAG Network ANR-08-PCVI-0023 and ANR Meca-GT ANR-13-BSV8-0011-01), a Royal Society International Joint Grant (to MWHC and SF-G), Grants from Région Lorraine and Lorraine University to SF-G and to NR, and was carried out under auspices of the International Associated Laboratory (*SFGEN*) funded between CNRS-UL (SF-G) and University of Dundee (J-CB and MWHC). Tayside Tissue Bank is supported by Breast Cancer Campaign, Cancer Research UK (CRUK), and by NHS Tayside through the Chief Scientist Office and Health Sciences Scotland (formerly the Scottish Academic Health Science Collaboration, AHSC).

Acknowledgments

Dr. Philippe Lassalle (INSERM U1019E11, Campus Institut Pasteur de Lille, Lille, France) is gratefully acknowledged for support with the xenograft experiments and for helpful discussion. Matthieu Chabel and Anne Robert are acknowledged for excellent technical assistance, and Xiaomeng Pang is acknowledged for performing methylation analysis.

REFERENCES

1 Bissell MJ, Hines WC. Why don't we get more cancer? A proposed role of the microenvironment in restraining cancer progression. *Nat Med* 2011; **17:** 320-329.

2 Breton C, Fournel-Gigleux S, Palcic MM. Recent structures, evolution and mechanisms of glycosyltransferases. *Curr Opin Struct Biol* 2012; **22:** 540-549.

3 Kusche-Gullberg M, Kjellen L. Sulfotransferases in glycosaminoglycan biosynthesis. *Curr Opin Struct Biol* 2003; **3:** 605-611.

4 Gulberti S, Lattard V, Fondeur M, Jacquinet JC, Mulliert G, Netter P, et al. Phosphorylation and sulfation of oligosaccharide substrates critically influence the activity of human beta 1,4-galactosyltransferase 7 (GalT-1) and beta 1,3-glucuronosyltransferase 1 (GlcAT-1) involved in the biosynthesis of the glycosaminoglycan-protein linkage region of proteoglycans. *J Biol Chem* 2005; **280:** 1417-1425.

5 Girardin EP, Hajmohammadi S, Birmele B, Helisch A, Shworak NW, de Agostini AI. Synthesis of anticoagulantly active heparan sulfate proteoglycans by glomerular epithelial cells involves multiple 3-*O*-sulfotransferase isoforms and a limiting precursor pool. *J Biol Chem* 2005; **280:** 38059-38070.

6 Shukla D, Liu J, Blaiklock P, Shworak NW, Bai X, Esko JD, et al. A novel role for 3-*O*-sulfated heparan sulfate in herpes simplex virus 1 entry. *Cell* 1999; **99:** 13-22.

7 Nurcombe V, Smart CE, Chipperfield H, Cool SM, Boilly B, Hondermarck H. The proliferative and migratory activities of breast cancer cells can be differentially regulated by heparan sulfates. *J Biol Chem* 2000; **275:** 30009-30018.

8 Lofgren L, Sahlin L, Jiang S, Von Schoultz B, Fernstad R, Skoog L, et al. Expression of syndecan-1 in paired samples of normal and malignant breast tissue from postmenopausal women. *Anticancer Res* 2007; **27:** 3045-3050.

9 Staub J, Chien J, Pan Y, Qian X, Narita K, Aletti G, et al. Epigenetic silencing of HSulf-1 in ovarian cancer: implications in chemoresistance. *Oncogene* 2007; **26:** 4969-4978.

10 Sasisekharan R, Shriver Z, Venkataraman G, Narayanasami U. Roles of heparan-sulphate glycosaminoglycans in cancer. *Nat Rev Cancer* 2002; **2:** 521-528.

11 Miyamoto K, Asada K, Fukutomi T, Okochi E, Yagi Y, Hasegawa T, et al. Methylation-associated silencing of heparan sulfate D-glucosaminyl 3-*O*-sulfotransferase-2 (3-OST2) in human breast, colon, lung and pancreatic cancers. *Oncogene* 2003; **22:** 274-280.

12 Raman K, Kuberan B. Chemical tumor biology of heparan sulfate proteoglycans. *Curr Chem Biol* 2010; **4:** 20-31.

13 Hwang JA, Kim Y, Hong SH, Lee J, Cho YG, Han JY, et al. Epigenetic inactivation of heparan sulfate (glucosamine) 3-*O*-sulfotransferase 2 in lung cancer and its role in tumorigenesis. *PLoS One* 2013; **8:** e79634.

14 Song K, Li Q, Jiang ZZ, Guo CW, Li P. Heparan sulfate D-glucosaminyl 3-O sulfotransferase-3B1, a novel epithelial-mesenchymal transition inducer in pancreatic cancer. *Cancer Biol Ther* 2011; **12:** 388-398.

15 Bui C, Ouzzine M, Talhaoui I, Sharp S, Prydz K, Coughtrie MW, et al. Epigenetics: methylation-associated repression of heparan sulfate 3-*O*-sulfotransferase gene expression contributes to the invasive phenotype of H-EMC-SS chondrosarcoma cells. *FASEB J* 2010; **24:** 436-450.

16 Goldhirsch A, Winer EP, Coates AS, Gelber RD, Piccart-Gebhart M, Thurlimann B, et al. Personalizing the treatment of women with early breast cancer: highlights of the St Gallen international expert consensus on the primary therapy of early breast cancer. *Ann Oncol* 2013; **24:** 2206-2223.
17 Di Croce L, Helin K. Transcriptional regulation by Polycomb group proteins. *Nat Struct Mol Biol* 2013; **10:** 1147-1155.
18 Fuks F, Hurd PJ, Wolf D, Nan X, Bird APKouzarides T. The methyl-CpG-binding protein MeCP2 links DNA methylation to histone methylation. *J Biol Chem* 2003; **278:** 4035-4040.
19 Kadamb R, Mittal S, Bansal N, Batra H, Saluja D. Sin3: insight into its transcription regulatory functions. *Eur J Cell Biol* 2013; **92:** 237-246.
20 van Kuppevelt TH, Dennissen MA, van Venrooij WJ, Hoet RM, Veerkamp JH. Generation and application of type-specific anti-heparan sulfate antibodies using phage display technology. Further evidence for heparan sulfate heterogeneity in the kidney. *J Biol Chem* 1998; **273:** 12960-12966.
21 Delehedde M, Lyon M, Sergeant N, Rahmoune H, Fernig DG. Proteoglycans: pericellular and cell surface multireceptors that integrate external stimuli in the mammary gland. *J Mammary Gland Biol Neoplasia* 2001; **6:** 253-273.
22 Ornitz DM, Xu J, Colvin JS, McEwen DG, MacArthur CA, Coulier F, et al. Receptor specificity of the fibroblast growth factor family. *J Biol Chem* 1996; **271:** 15292-15297.
23 Kitsberg DI, Leder P. Keratinocyte growth factor induces mammary and prostatic hyperplasia and mammary adenocarcinoma in transgenic mice. *Oncogene* 1996; **13:** 2507-2515.
24 Jacquemier J, Sun ZZ, Penault-Llorca F, Geneix J, Devilard E, Adelaide J, et al. FGF7 protein expression in human breast carcinomas. *J Pathol* 1998; **86:** 269-274.
25 Zang XP, Siwak DR, Nguyen TX, Tari AM, Pento JT. KGF-induced motility of breast cancer cells is dependent on Grb2 and Erk1,2. *Clin Exp Metastasis* 2004; **21:** 437-443.
26 Cha JY, Lambert QT, Reuther GW, Der CJ. Involvement of fibroblast growth factor receptor isoform switching in mammary oncogenesis. *Mol Cancer Res* 2008; **6:** 435-445.
27 Turner N, Grose R. Fibroblast growth factor signalling: from development to cancer. *Nat Rev Cancer* 2010; **10:** 116-129.
28 Marcel V, Fernandes K, Terrier O, Lane DP, Bourdon JC. Modulation of p53beta and p53gamma expression by regulating the alternative splicing of TP53 gene modifies cellular response. *Cell Death Differ* 2014; **21:** 1377-1387.
29 Hajian-Tilaki K. Receiver operating characteristic (ROC) curve analysis for medical diagnostic test evaluation. *Caspian J Intern Med* 2013; **4:** 627-635.
30 Budczies J, Klauschen F, Sinn BV, Gyorffy B, Schmitt WD, Darb-Esfahani S, et al. Cutoff finder: a comprehensive and straightforward Web application enabling rapid biomarker cutoff optimization. *PLoS One* 2012; **7:** e51862.
31 Thacker BE, Xu D, Lawrence R, Esko JD. Heparan sulfate 3-*O*-sulfation: a rare modification in search of a function. *Matrix Biol* 2013; **35:** 60-72.
32 Kokura K, Sun L, Bedford MT, Fang J. Methyl-H3K9-binding protein MPP8 mediates E-cadherin gene silencing and promotes tumour cell motility and invasion. *EMBO J* 2010; **29:** 3673-3687.

33 Kloten V, Becker B, Winner K, Schrauder MG, Fasching PA, Anzeneder T, et al. Promoter hypermethylation of the tumor-suppressor genes ITIH5, DKK3, and RASSF1A as novel biomarkers for blood-based breast cancer screening. *Breast Cancer Res* 2013; **15:** R4.

34 Hervouet E, Cartron PF, Jouvenot M, Delage-Mourroux R. Epigenetic regulation of estrogen signaling in breast cancer. *Epigenetics* 2013; **8:** 237-245.

35 Shukla S, Mirza S, Sharma G, Parshad R, Gupta SD, Ralhan R. Detection of RASSF1A and RARbeta hypermethylation in serum DNA from breast cancer patients. *Epigenetics* 2006; **1:** 88-93.

36 Dieci MV, Arnedos M, Andre F, Soria JC. Fibroblast growth factor receptor inhibitors as a cancer treatment: from a biologic rationale to medical perspectives. *Cancer Discov* 2013; **3:** 264-279.

37 Cha JY, Maddileti S, Mitin N, Harden TK, Der CJ. Aberrant receptor internalization and enhanced FRS2-dependent signaling contribute to the transforming activity of the fibroblast growth factor receptor 2 IIIb C3 isoform. *J Biol Chem* 2009; **284:** 6227-6240

38 Bai A, Meetze K, Vo NY, Kollipara S, Mazsa EK, Winston WM, et al. GP369, an FGFR2-IIIb-specific antibody, exhibits potent antitumor activity against human cancers driven by activated FGFR2 signaling. *Cancer Res* 2010; **70:** 7630-7639.

39 Ye S, Luo Y, Lu W, Jones RB, Linhardt RJ, Capila I, et al. Structural basis for interaction of FGF-1, FGF-2, and FGF-7 with different heparan sulfate motifs. *Biochemistry* 2001; **40:** 14429-14439

40 Xu R, Ori A, Rudd TR, Uniewicz KA, Ahmed YA, Guimond SE, et al. Diversification of the structural determinants of fibroblast growth factor-heparin interactions: implications for binding specificity. *J Biol Chem* 2012; **287:** 40061-40073.

41 Mehta M, Kesinger JW, Zang XP, Lerner ML, Brackett DJ, Brueggemeier RW, et al. Influence of novel KGFR tyrosine kinase inhibitors on KGF-mediated proliferation of breast cancer. *Anticancer Res* 2010; **30:** 4883-4889.

42 Luo Y, Ye S, Kan M, McKeehan WL. Control of fibroblast growth factor (FGF) 7- and FGF1-induced mitogenesis and downstream signaling by distinct heparin octasaccharide motifs. *J Biol Chem* 2006; **281:** 21052-21061.

43 Nieto L, Canales Á, Fernández IS, Santillana E, González-Corrochano R, Redondo-Horcajo M, et al. Heparin modulates the mitogenic activity of fibroblast growth factor by inducing dimerization of its receptor. a 3D view by using NMR. *Chembiochem* 2013; **14:** 1732-1744.

44 Fournel-Gigleux S, Sutherland L, Sabolovic N, Burchell B, Siest G. Stable expression of two human UDP-glucuronosyltransferases cDNAs in V79 cell cultures. *Mol Pharmacol* 1991; **39:** 177-183.

45 Bourdon JC, Khoury MP, Diot A, Baker L, Fernandes K, Aoubala M, et al. p53 mutant breast cancer patients expressing p53gamma have as good a prognosis as wild-type p53 breast cancer patients. *Breast Cancer Res* 2011; **13:** R7.

46 Bloom HJ, Richardson WW. Histological grading and prognosis in breast cancer; a study of 1409 cases of which 359 have been followed for 15 years. *Br J Cancer* 1957; **11:** 359-377.

47 Detre S, Saclani Jotti G, Dowsett M. A "quickscore" method for immunohistochemical semiquantitation: validation for oestrogen receptor in breast carcinomas. *J Clin Pathol* 1995; **48:** 876-878.

48 Purdie CA, Jordan LB, McCullough JB, Edwards SL, Cunningham J, Walsh M, et al. HER2 assessment on core biopsy specimens using monoclonal antibody CB11 accurately determines HER2 status in breast carcinoma. *Histopathology* 2010; **56:** 702-707.

Figure Legends

Figure 1. *3-OST3A* gene expression is regulated by DNA methylation and histone deacetylation in breast cancer cells. **A,** 3-OST3A mRNA expression level is differentially repressed in breast cancer cell lines representative of different subtypes of tumors. RT-qPCR was performed using gene-specific primers, expression level was normalized to *RP29,* and mRNA level in breast cancer cell lines is expressed relative to MCF-10A control cells (set to 1). ***P*<0.01, ****P*<0.001, n=3. **B,** the methylation profile of the proximal promoter region (5') and first exon (3') of *3-OST3A* shows hypermethylation in all cell lines but SKBR3. The number of methylated and non-methylated sites in the regions of interest (shown in Fig. S1) is indicated by hatched and empty bars, respectively. Results are the mean from sequencing data of at least 3 independent clones. **C,** effect of the DNAmethyltransferase inhibitor Aza, and of the histone deacetylase inhibitor TSA on 3-OST3A mRNA expression level indicate epigenetic mechanisms involving DNA methylation and histone deacetylation. MCF-7 (left panel) or MDA-MB-231 cells (right panel) were treated with Aza or TSA alone, or with both drugs. RT-qPCR was performed as described in panel A. ***P*<0.01, ****P*<0.001, n=3.

Figure 2. Distinct epigenetic marks are associated with the *3-OST3A* gene in breast cancer cells. **A,** a representative map of the *3-OST3A* gene with ChIP-PCR primers indicated below. Three sets of primers (p1-p3) covering the CpG island of the *3-OST3A* gene were used for PCR amplification. Location to TSS, *p1:* -347 to -129; *p2:* +216 to +393; *p3:* +468 to +605. Amount of (**B**) DNMT isoforms, (**C**) H3K4me3, H3K9me3 and H3K27me3 marks, (**D**) EZH2 and SUZ12 of PRC2 complex, (**E**) HDAC1, MeCP2 and Sin3A recruited at the *3-OST3A* gene using specific antibodies was compared to input (about 2% total chromatin) and IgG negative control in MCF-10A, MCF-7 and MDA-MB-231 cells. **F**, schematic representation of chromatin regulators at the *3-OST3A* gene. In MCF-7 cells, DNMT3B, EZH2 and H3K27me3 mediates moderate transcriptional repression independently from MeCP2 and HDAC1, while in MDA-MB-231, DNMTs are closely connected to HDAC1 *via* MeCP2 and Sin3A in a strong repressive complex.

Figure 3. 3-OST3A expression or silencing produces contrasting effects on cell proliferation in different breast cancer cells. **A**, cell proliferation assessed in breast cancer cell lines 1 to 5 days following transient transfection with empty pcDNA vector (control) or 3-OST3A-HA cDNA (3-OST3A) was reduced in MCF-7 and MDA-MB-231 but enhanced in SKBR3 cells. 3-OST3A expression was monitored by immunoblot analysis using anti-HA antibodies (shown below histograms). SKBR3 cells transfected with siRNA control or 3-OST3A siRNA showed reduced cell growth in depleted cells. **P*<0.05, ***P*<0.01, ****P*<0.001, n=4. **B**, cell growth rate was assessed 2 days following transient transfection with 3-OST3A-HA cDNA, siRNA and corresponding controls in SKBR3 cells, as in panel A, and treated with 0, 20 and 40 µg/mL trastuzumab. The antiproliferative effect of trastuzumab was enhanced upon 3-OST3A expression whereas it was suppressed in SKBR3-depleted cells. ***P*<0.01, ****P*<0.001, n=4.

Figure 4. 3-OST3A expression triggers apoptotic events in MCF-7 cells and retards tumor growth in xenografted mice. **A**, Annexin V assay in MCF-7 cells transiently transfected with empty vector (control) or 3-OST3A cDNA (3-OST3A) by FACS analysis (left panel). Quantitative analysis of early (annexin V+/PI-, right low square) and late (annexinV+/PI+, right upper square) stages of apoptosis shows increased percentage of apoptotic cells upon 3-OST3A expression (right panel). ***P*<0.01,

n=3. **B**, immunoblot analysis of apoptotic proteins in MCF-7 cells transfected with empty vector (control) or 3-OST3A cDNA (3-OST3A). Quantitative analysis of protein expression using Image J software shows increased Bax and decreased Bcl2 level, and increased cleaved caspase 9 and cleaved PARP. Expression level of each protein is expressed relative to control cells (set to 1). ***P*<0.01, n=3. **C**, TUNEL assay in MCF-7 cells transfected with empty vector (control) or 3-OST3A cDNA (3-OST3A) by dUTP labelling shows increased DNA fragmentation. Quantitative analysis of fragmented DNA was performed using Image J software. Level of fragmented DNA is expressed relative to control cells (set to 1). ****P*<0.001, n=3. Scale = 25 µm. **D**, 3-OST3A expression in pcDNA (Control-A and B) and 3-OST3A-HA (3-OST3A-A and B) stably transfected MCF-7 cells were analyzed by immunoblotting after 10 passages. **E** and **F**, the effect of 3-OST3A in 3-OST3A-A and -B MCF-7 cell lines compared with tumors formed in mice implanted with Control-A and -B shows delayed tumor formation. Controls are represented by black solid circles and 3-OST3A-expressing cells by red solid circles. **P*<0.05, ***P*<0.01, n=3 or 4.

Figure 5. 3-OST3A expression impairs FGF-7 cell-surface binding *via* FGF-7-HS interactions and regulates FGF-7-dependent signaling in MCF-7 cells. **A**, confocal immunofluorescence microscopy of FGF-7 cell-surface binding on MCF-10A cells transfected by siRNA control or siRNA 3-OST3A (upper panel) and on MCF-7 cells transfected with empty vector (control) or with 3-OST3A cDNA (3-OST3A) (lower panel). Cells were doubled-stained for bound FGF-7 (green) and nucleus (blue). A single cell is presented in inset. **B**, semi-quantitative analysis of the fluorescence intensity from panel A using Image J software shows increased FGF-7 binding in 3-OST3A siRNA depleted MCF-10A cells and reduced FGF-7 binding upon 3-OST3A expression in MCF-7 cells. ****P*<0.001, n=3. **C**, flow cytometry of FGF-7 cell-surface binding performed on cells transfected as in panel A. Upper panel shows increased fluorescence signal in MCF-10A transfected by siRNA 3-OST3A (green) compared to siRNA control (white). Lower panel shows reduced fluorescence signal in MCF-7 transfected with 3-OST3A cDNA (green) compared with empty vector (white). **D**, FRET analysis of FGF-7-HS interactions using anti-FGF-7-AlexaFluor 488 antibodies as fluorescence donor, in the presence of anti-HS-AlexaFluor 555 antibodies as acceptor. Quantification of FRET by FLIM showing the distribution of lifetime of the donor from 0.25 (orange, FRET++) to 2.1 ns (blue, FRET-) indicates more FRET positive cells (green) in control compared to 3-OST3A cells. **E,** lifetime decay showed higher average lifetime of donor in 3-OST3A cells compared to HA-negative and empty vector transfected cells (shown in Table 1 and Fig. S4). **F, G, H,** 3-OST3A expression regulates FGF-7-mediated signaling. 3-OST3A transfected MCF-7 cells were serum-starved for 24 h and treated with FGF-7. Lower panels show a representative immunoblot of cell lysates performed with (**F**) anti-phospho-AKT and anti-AKT, (**G**) anti-phospho-ERK1/2 and anti-ERK1/2, and (**H**) anti-phospho-p38 and anti-p38 antibodies. The relative intensity of immunoreactive bands of phosphorylated versus total protein shown in upper panels. **P*<0.05, n=3.

Figure 6. 3-OST3A expression depends on the breast cancer subtype and determines clinical outcome. **A**, multi-variable Kruskal-Wallis non-parametric test was used to analyse the association between the breast cancer subtype (triple negative (TN, ER-,PR-,HER2-), luminal B (lumB, ER+, PR-, HER2-), luminal A (lumA, ER+,PR+,HER2-), HER2+ (HER2+ regardless of ER and PR status)) and 3-OST3A expression level determined by RT-qPCR. **B**, non-parametric Kaplan-Meier plots shows that disease-free survival (left) and cancer-related survival (right) in HER2+ patients was significantly lower in 3-OST3A positive tumors. **C**, non-parametric Kaplan-Meier plots of binary variable (3ost, S, LN) in relation to disease-free survival (left) and cancer-related survival (right) shows that 71% positive patients suffered from recurrence and among them 60% from death. Censored cases are shown on the curves. Log-rank analyses and *P* values are indicated. The number of patients (n) and events (e) are indicated.

Table 1. Lifetime of FGF-7-AlexaFluor 488 in MCF-7 cells

Condition	Lifetime (ns)
3-OST3A cDNA	0.95 ± 0.07*†
HA-	0.36 ± 0.12*
Control cDNA	0.42 ± 0.10

3-OST3A cDNA, HA-negative (HA-) and control cDNA correspond to regions analyzed in 3-OST3A cDNA-transfected cells expressing 3-OST3A-HA, in 3-OST3A cDNA-transfected cells lacking 3-OST3A-HA expression and in empty vector-transfected cells, respectively, as in Fig. S4A and B. Data are mean ± SEM. *P<0.05 *vs*. control cDNA, †P<0.05 *vs*. HA-, n=3. Statistical analysis was performed using one-way ANOVA with Tukey's post-hoc test.

Table 2. Multivariate Cox's regression analysis on primary HER2+ breast cancer

	Itr.	Predictor	Omnibus test of model coefficient			HR	95% CI	
			χ^2	df	I value			
Disease-free survival	1	(3ost, S, LN)	23.233	1	2.10^{-6}	27.3	3.6	207.7
Overall survival	1	(3ost, S, LN)	14.354	1	2.10^{-4}	117.1	0.41	3.10^{5}

Number of HER2+ patients, 49. The clinico-pathological parameters were: presence of lymph node metastasis (LN), tumor size (S), 3-OST3A (3ost) and the combined binary variable (3ost, S, LN). HR, hazard ratio; CI, confidence interval.

Figure 1

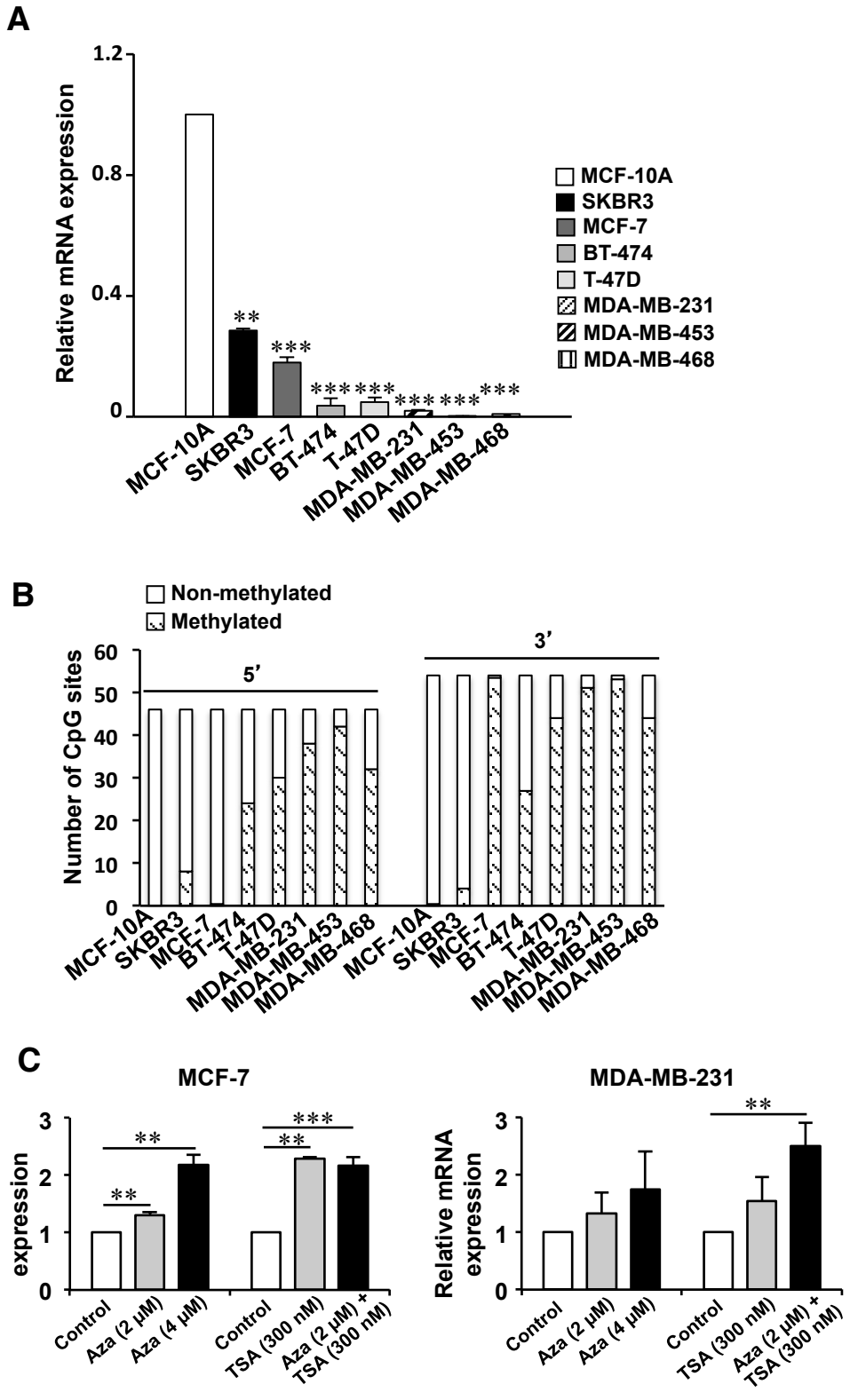
A
Relative mRNA expression
1.2
0.8
0.4
0
MCF-10A
SKBR3
MCF-7
BT-474
T-47D
MDA-MB-231
MDA-MB-453
MDA-MB-468
B
Non-methylated
Methylated
Number of CpG sites
60
50
40
30
20
10
0
5'
3'
C
MCF-7
MDA-MB-231
Relative mRNA expression
Control
Aza (2 μM)
Aza (4 μM)
TSA (300 nM)
Aza (2 μM) + TSA (300 nM)

Figure 2

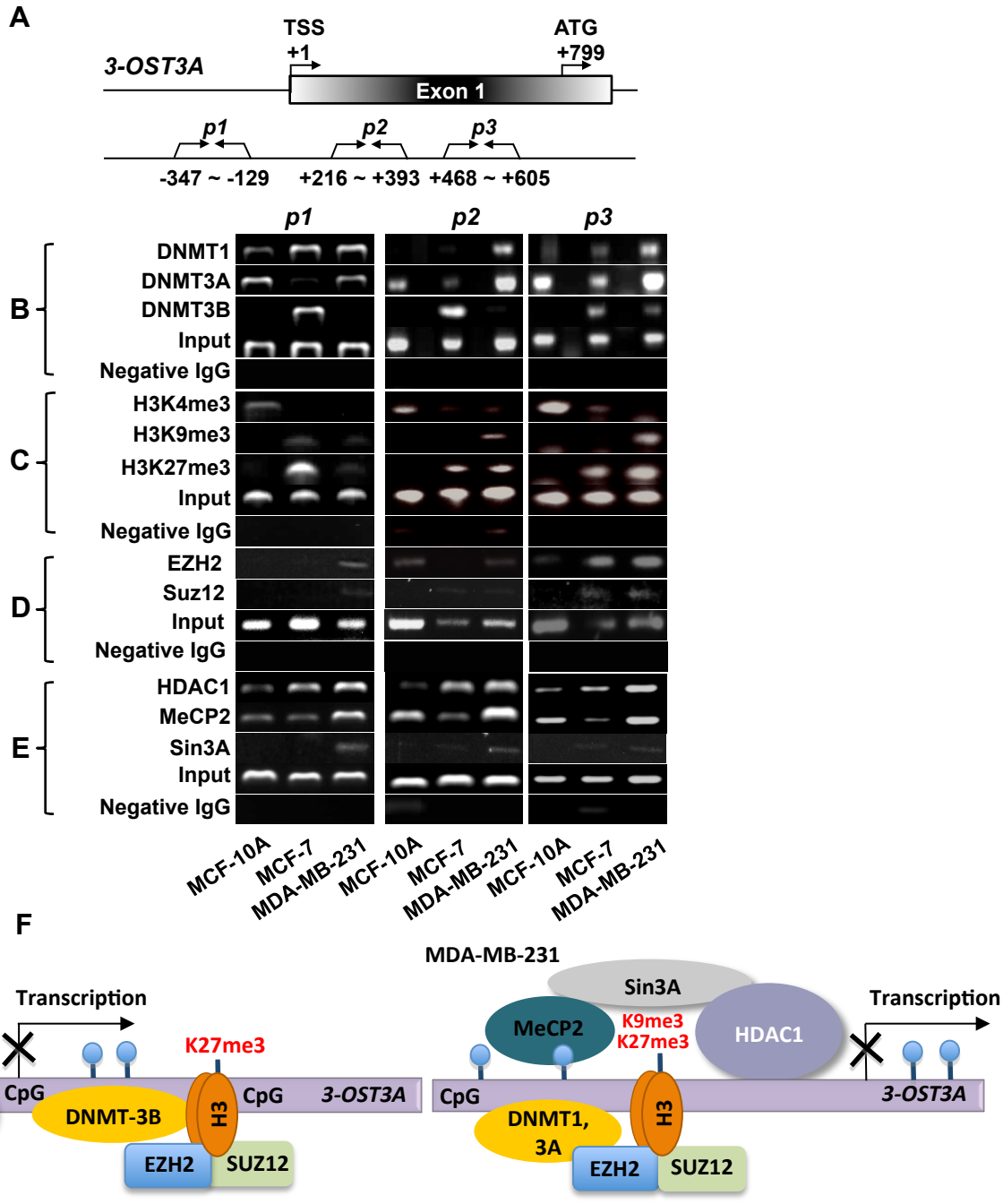
A
TSS
+1
ATG
+799
3-OST3A
Exon 1
p1
p2
p3
-347 ~ -129
+216 ~ +393
+468 ~ +605
p1
p2
p3
B
DNMT1
DNMT3A
DNMT3B
Input
Negative IgG
C
H3K4me3
H3K9me3
H3K27me3
Input
Negative IgG
D
EZH2
Suz12
Input
Negative IgG
E
HDAC1
MeCP2
Sin3A
Input
Negative IgG
MCF-10A
MCF-7
MDA-MB-231
MCF-10A
MCF-7
MDA-MB-231
MCF-10A
MCF-7
MDA-MB-231
F
MCF-7
Transcription
K27me3
HDAC1
CpG
DNMT-3B
H3
CpG
3-OST3A
EZH2
SUZ12
MDA-MB-231
Sin3A
MeCP2
K9me3
K27me3
HDAC1
Transcription
CpG
DNMT1,
3A
H3
3-OST3A
EZH2
SUZ12

Figure 3

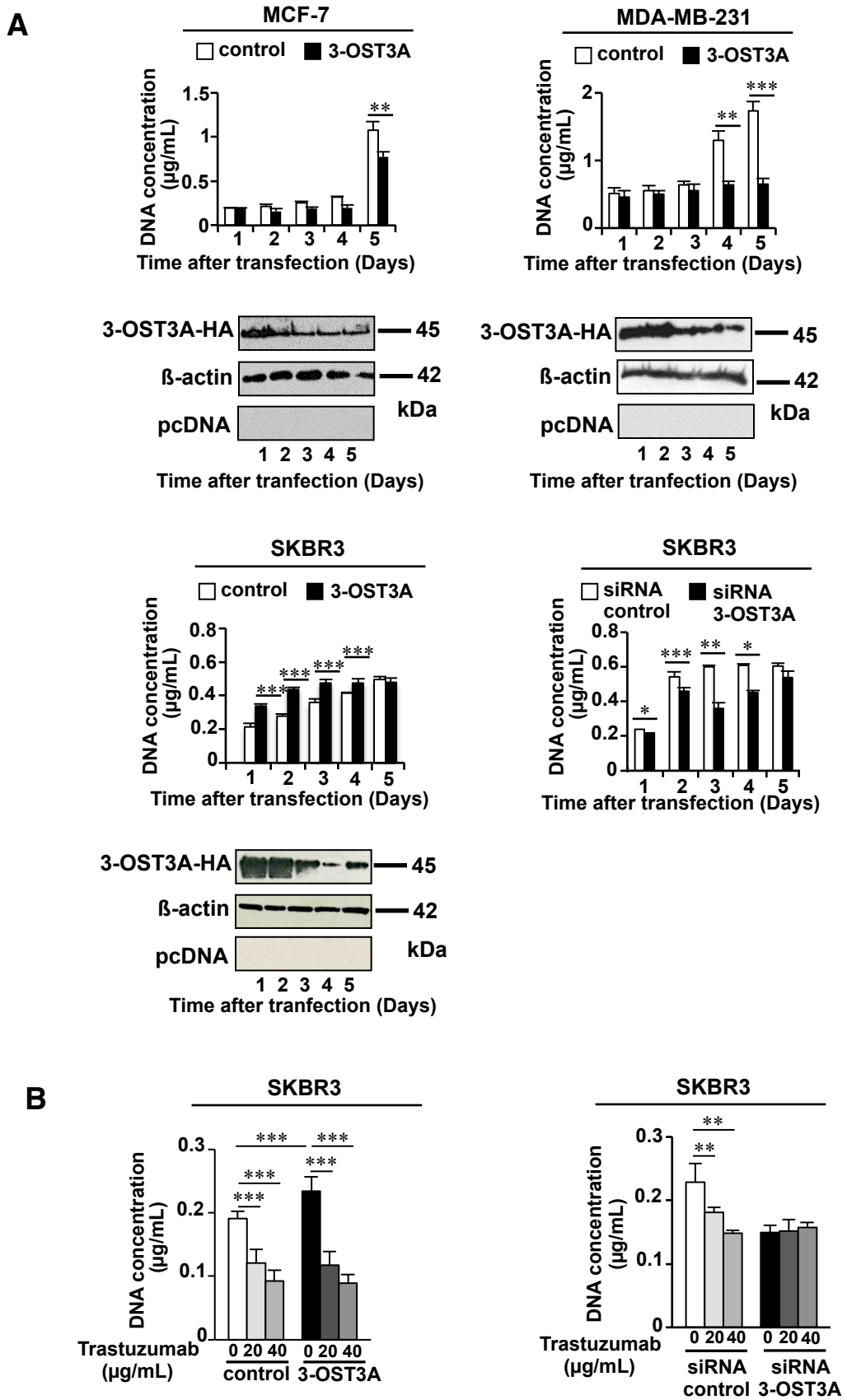
A
MCF-7
control
3-OST3A
DNA concentration (µg/mL)
Time after transfection (Days)
MDA-MB-231
3-OST3A-HA
ß-actin
pcDNA
45
42
kDa
Time after tranfection (Days)
SKBR3
siRNA control
siRNA 3-OST3A
B
Trastuzumab (µg/mL)
0 20 40

Figure 4

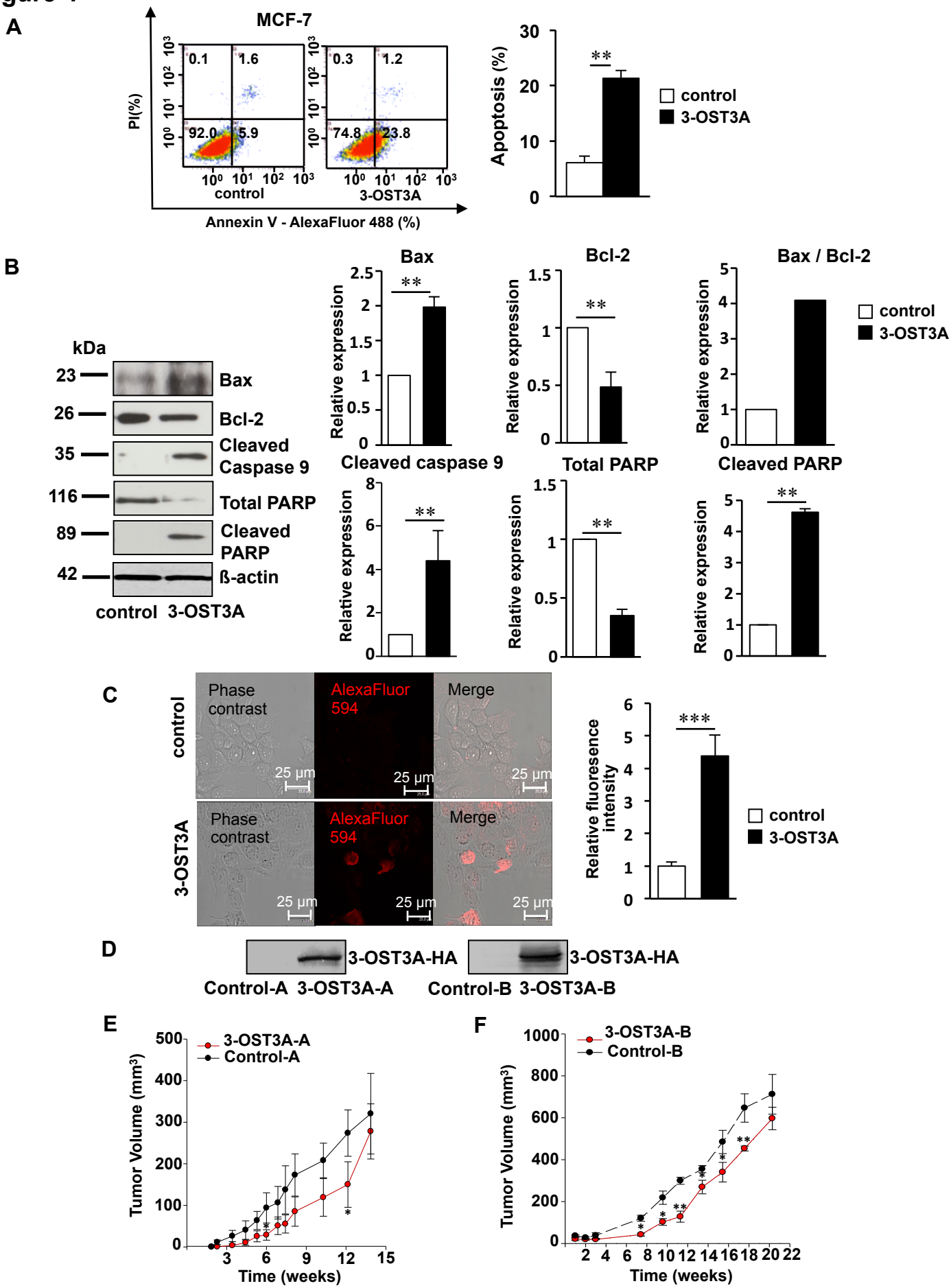
A
MCF-7
PI(%)
Annexin V - AlexaFluor 488 (%)
0.1
1.6
92.0
5.9
control
0.3
1.2
74.8
23.8
3-OST3A
Apoptosis (%)
control
3-OST3A
B
kDa
23
Bax
26
Bcl-2
35
Cleaved Caspase 9
116
Total PARP
89
Cleaved PARP
42
ß-actin
control 3-OST3A
Bax
Bcl-2
Bax / Bcl-2
Relative expression
Cleaved caspase 9
Total PARP
Cleaved PARP
C
control
3-OST3A
Phase contrast
AlexaFluor 594
Merge
25 µm
Relative fluoresence intensity
D
3-OST3A-HA
Control-A 3-OST3A-A
Control-B 3-OST3A-B
E
3-OST3A-A
Control-A
Tumor Volume (mm³)
Time (weeks)
F
3-OST3A-B
Control-B
Tumor Volume (mm³)
Time (weeks)

Figure 5

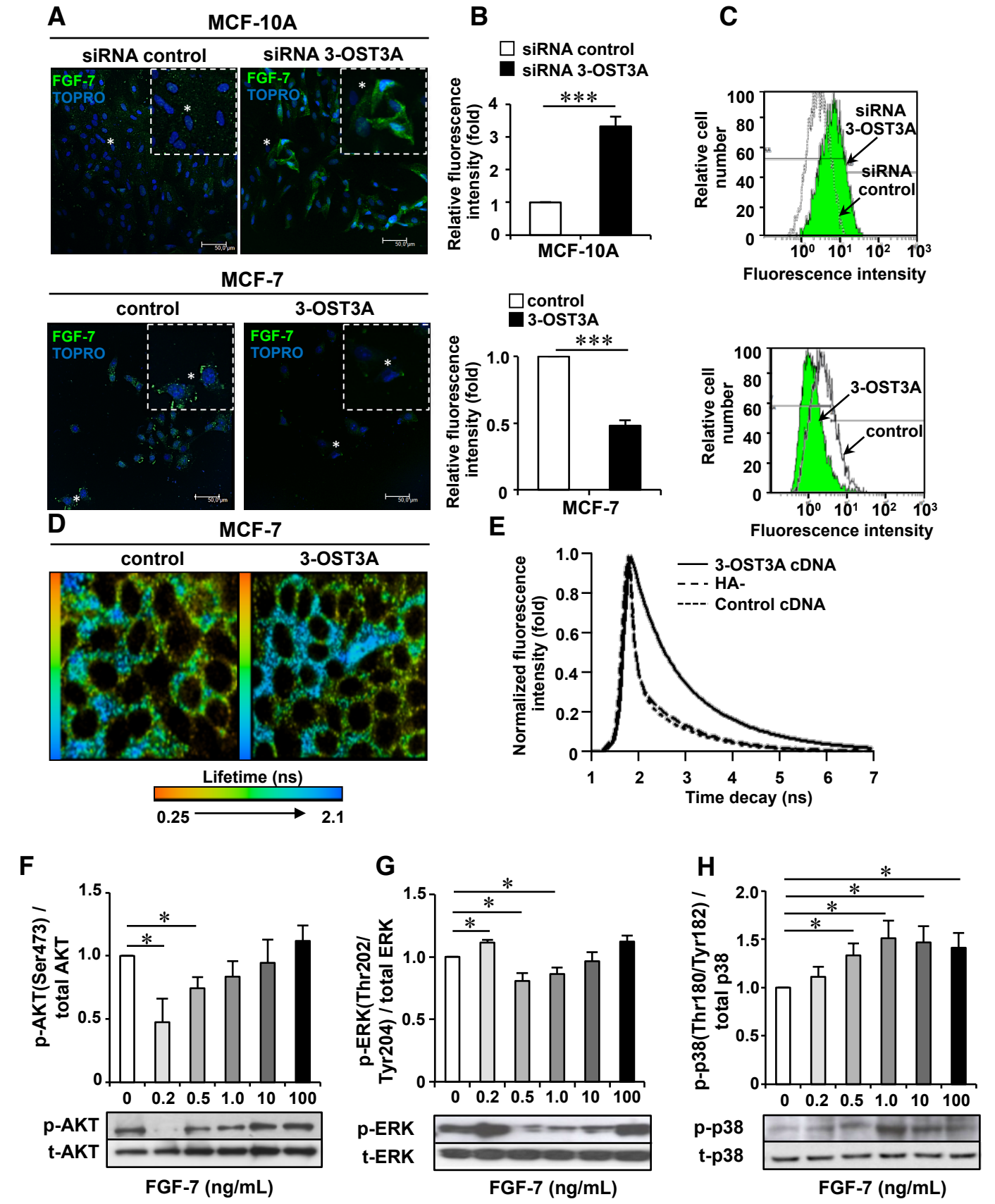
A
MCF-10A
siRNA control
siRNA 3-OST3A
FGF-7
TOPRO
MCF-7
control
3-OST3A
B
siRNA control
siRNA 3-OST3A
Relative fluorescence intensity (fold)
***
MCF-10A
control
3-OST3A
MCF-7
C
Relative cell number
siRNA 3-OST3A
siRNA control
Fluorescence intensity
3-OST3A
control
D
Lifetime (ns)
0.25
2.1
E
Normalized fluorescence intensity (fold)
3-OST3A cDNA
HA-
Control cDNA
Time decay (ns)
F
p-AKT(Ser473) / total AKT
p-AKT
t-AKT
FGF-7 (ng/mL)
G
p-ERK(Thr202/ Tyr204) / total ERK
p-ERK
t-ERK
FGF-7 (ng/mL)
H
p-p38(Thr180/Tyr182) / total p38
p-p38
t-p38
FGF-7 (ng/mL)

Figure 6

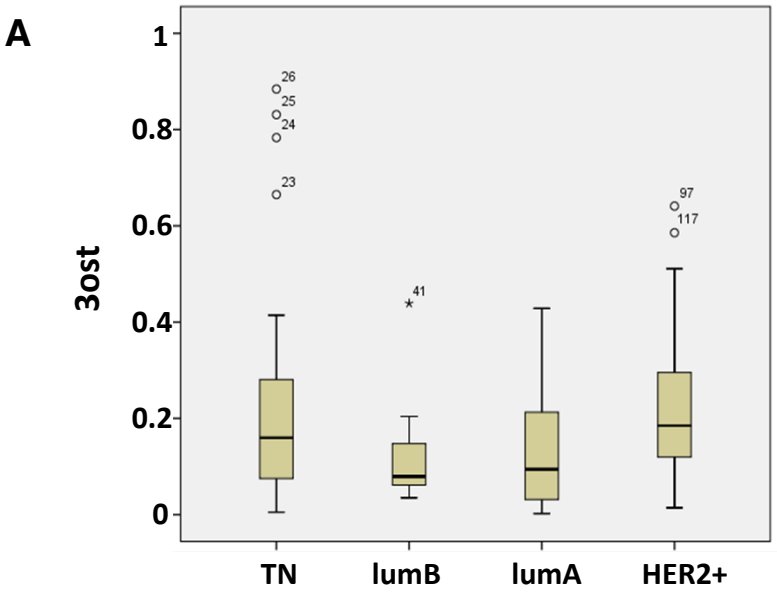
A
3ost
1
0.8
0.6
0.4
0.2
0
26
25
24
23
41
97
117
TN
lumB
lumA
HER2+

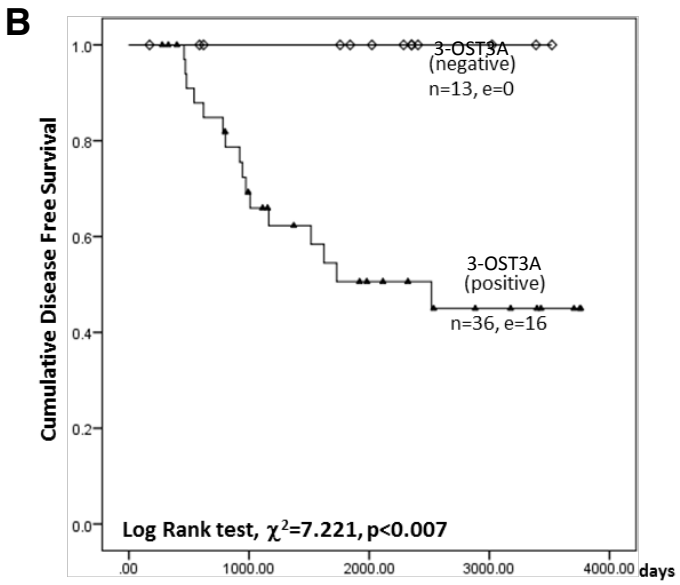
B
Cumulative Disease Free Survival
3-OST3A (negative)
n=13, e=0
3-OST3A (positive)
n=36, e=16
Log Rank test, χ^2=7.221, p<0.007
.00
1000.00
2000.00
3000.00
4000.00
days

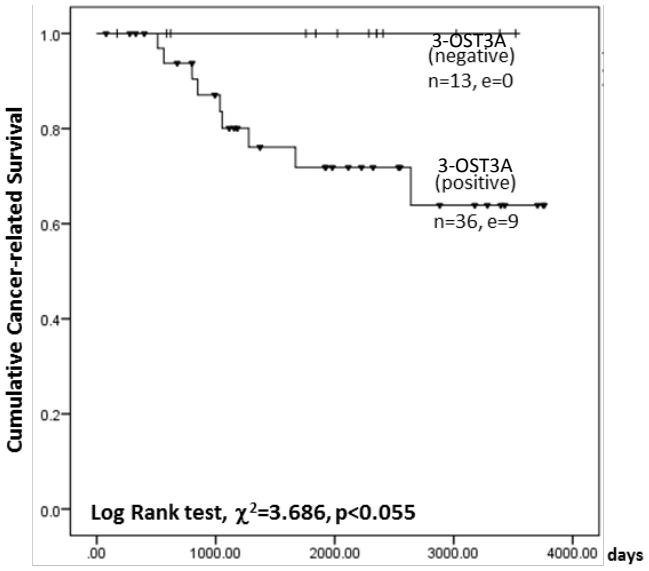
Cumulative Cancer-related Survival
3-OST3A (negative)
n=13, e=0
3-OST3A (positive)
n=36, e=9
Log Rank test, χ^2=3.686, p<0.055
.00
1000.00
2000.00
3000.00
4000.00
days

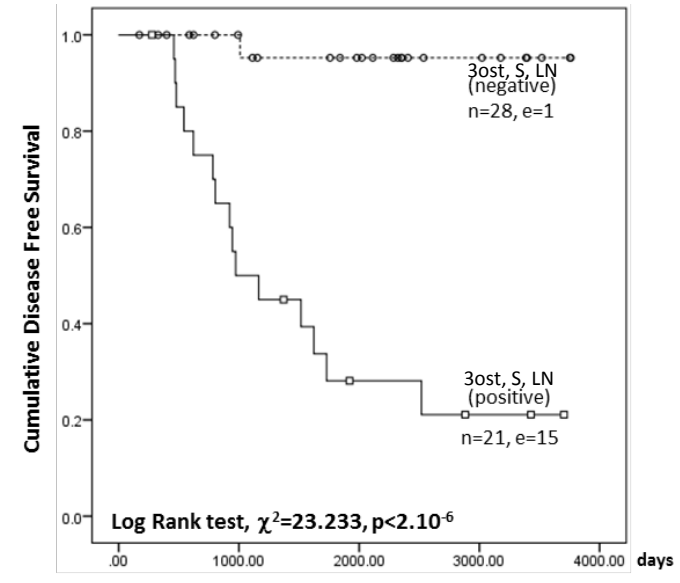
C
Cumulative Disease Free Survival
3ost, S, LN (negative)
n=28, e=1
3ost, S, LN (positive)
n=21, e=15
Log Rank test, χ^2=23.233, p<2.10^{-6}
.00
1000.00
2000.00
3000.00
4000.00
days

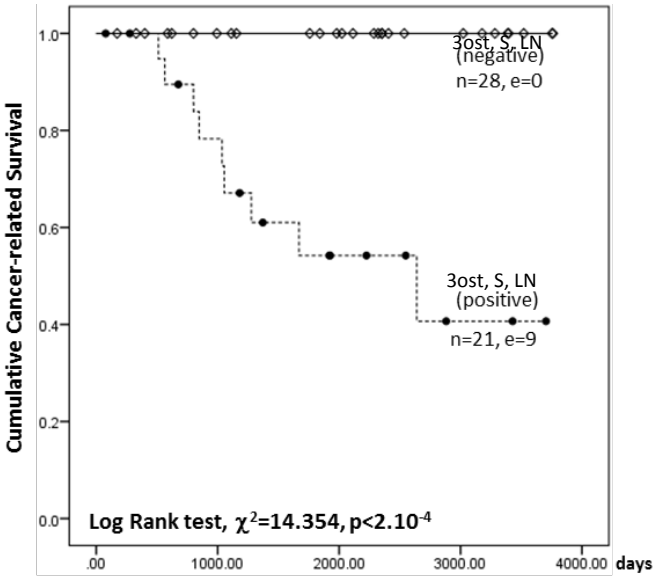
Cumulative Cancer-related Survival
3ost, S, LN (negative)
n=28, e=0
3ost, S, LN (positive)
n=21, e=9
Log Rank test, χ^2=14.354, p<2.10^{-4}
.00
1000.00
2000.00
3000.00
4000.00
days

Figure S1

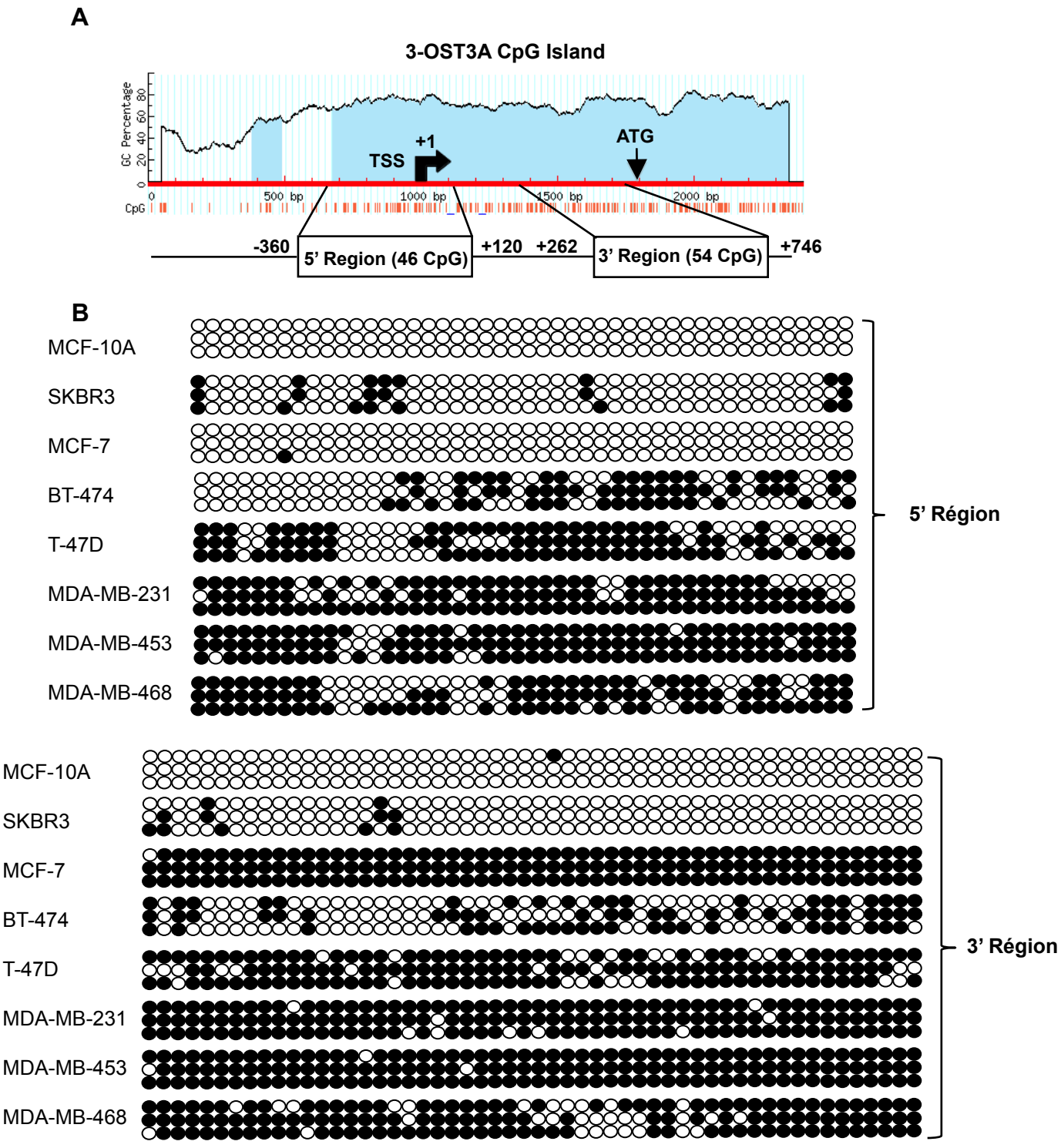

Figure S1. Hypermethylation of *3-OST3A* gene in breast cancer cell lines. **A**, analysis of the human *3-OST3A* gene sequence for the presence of a CpG island (shown in blue) using MethPrimer software. Two sequences were analyzed *i.e.* the proximal promoter region (indicated as 5' region) and a region containing the first transcribed exon (indicated as 3' region), located at -360 to +120 and at +262 to +746 to the TSS, respectively. Red vertical lines below the diagram indicate the CpG sites, the TSS is marked by a black curved arrow and the ATG is shown by an arrow**. B**, methylation profile of the two regions of interest in MCF-10A, SKBR3, MCF-7, BT-474, T-47D, MDA-MB-231, MDA-MB-453 and MDA-MB-468 cells. Circles represent the total number of CpG sites in the 5' and 3' regions (46 and 54, respectively). Open and solid circles depict the unmethylated and methylated CpG sites, respectively. Results show bisulfite sequencing of 3 different clones.

Figure S2

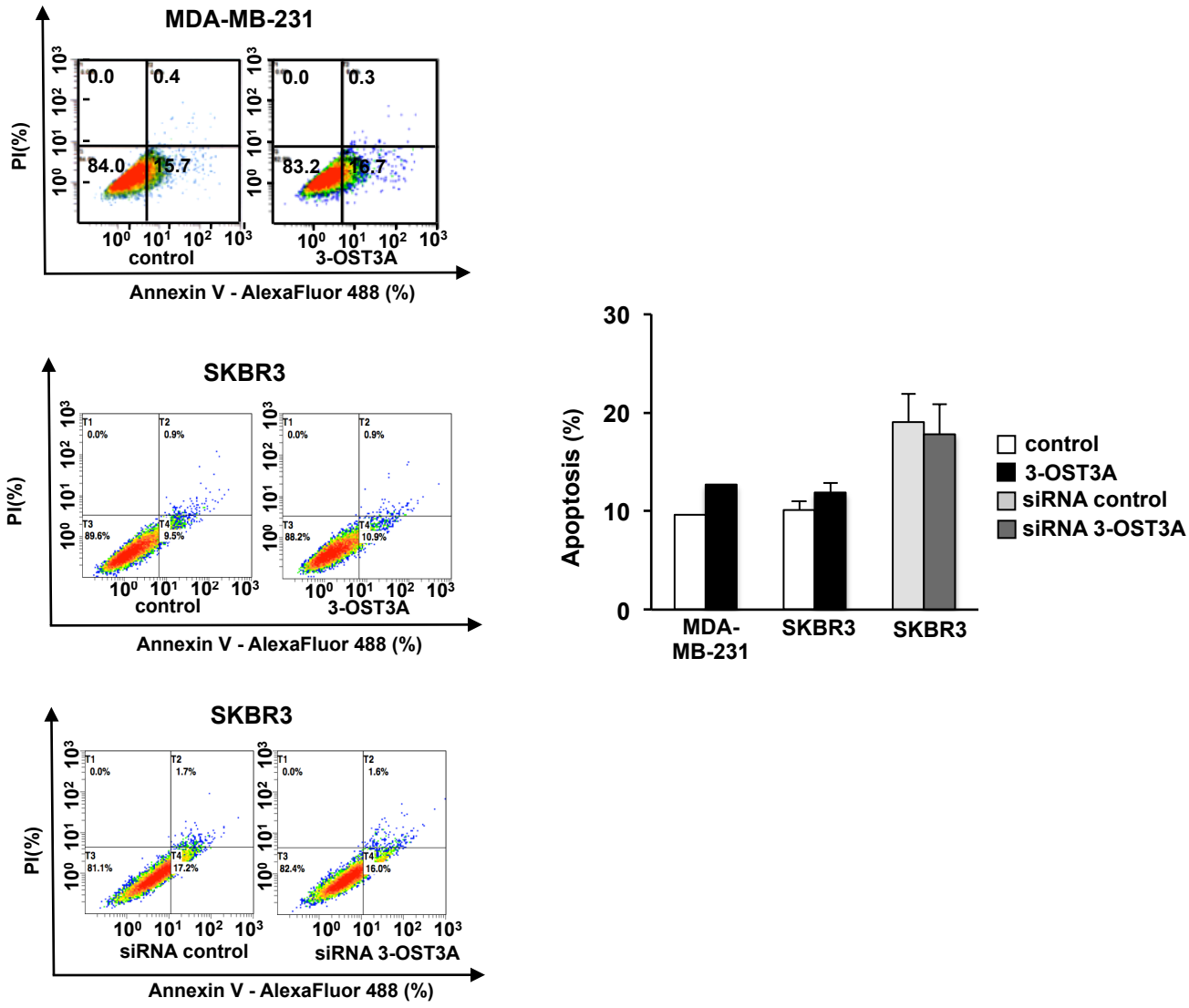

Figure S2. Effect of 3-OST3A overexpression and knockdown on apoptosis determined by Annexin V flow cytometry assay. Forty-eight hours following transient transfection with 3-OST3A cDNA or with siRNA 3-OST3A and controls, cells were analyzed by flow cytometry. Representative profile from 10,000 events per sample shows Annexin V-AlexaFluor 488 staining (*x* axis) and PI staining (*y* axis). Cells were classified as healthy cells (Annexin V−, PI−, left lower square), early apoptotic cells (Annexin V+, PI−, right lower square), late apoptotic cells (Annexin V+, PI+, right upper square), and damaged cells (Annexin V−, PI+, left upper square). Quantitative analysis of early (annexin V+/PI-) and late (annexinV+/PI+) stages of apoptosis was performed. Data are expressed as percentage of apoptotic (early and late) to total number of cells.

Figure S3

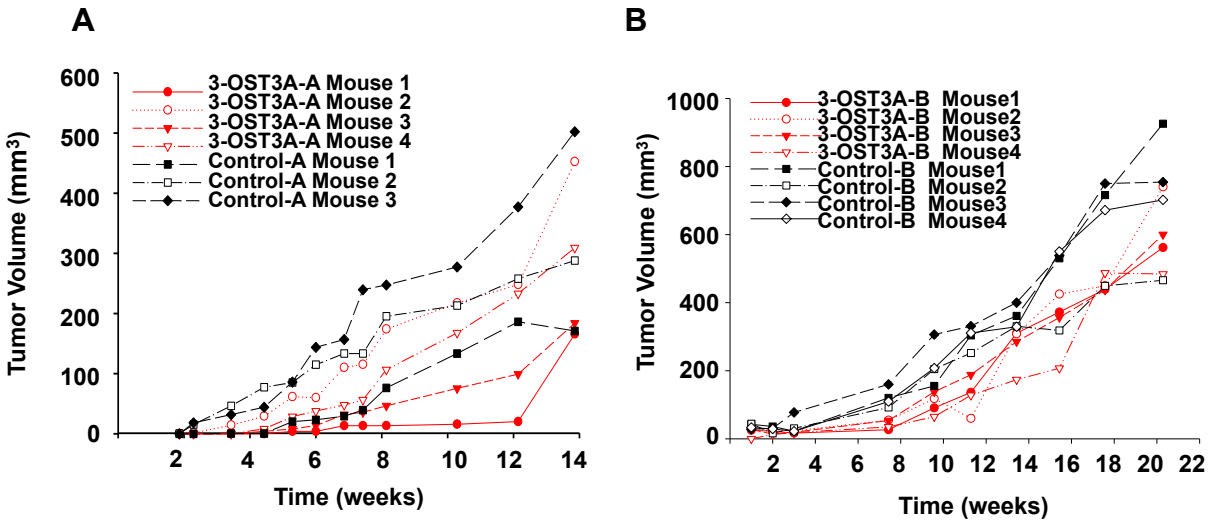

Figure S3. The tumor suppressor effect of 3-OST3A cDNA stably transfected in MCF-7 cells (3-OST3A-A and -B) was evaluated in SCID mice compared with tumors formed from MCF-7 cells stably transfected with their empty vector (Control-A and -B). Mice were injected with 5×10^6 control cells (black solid and dotted lines) or 3-OST3A expressing cells (red solid and dotted lines) and tumor size was measured up to 14 and 20 weeks in two separate experiments (panels **A** and **B**). In experiment shown in panel A, one mouse in control group did not develop any tumor and was omitted from the figure.

Figure S4

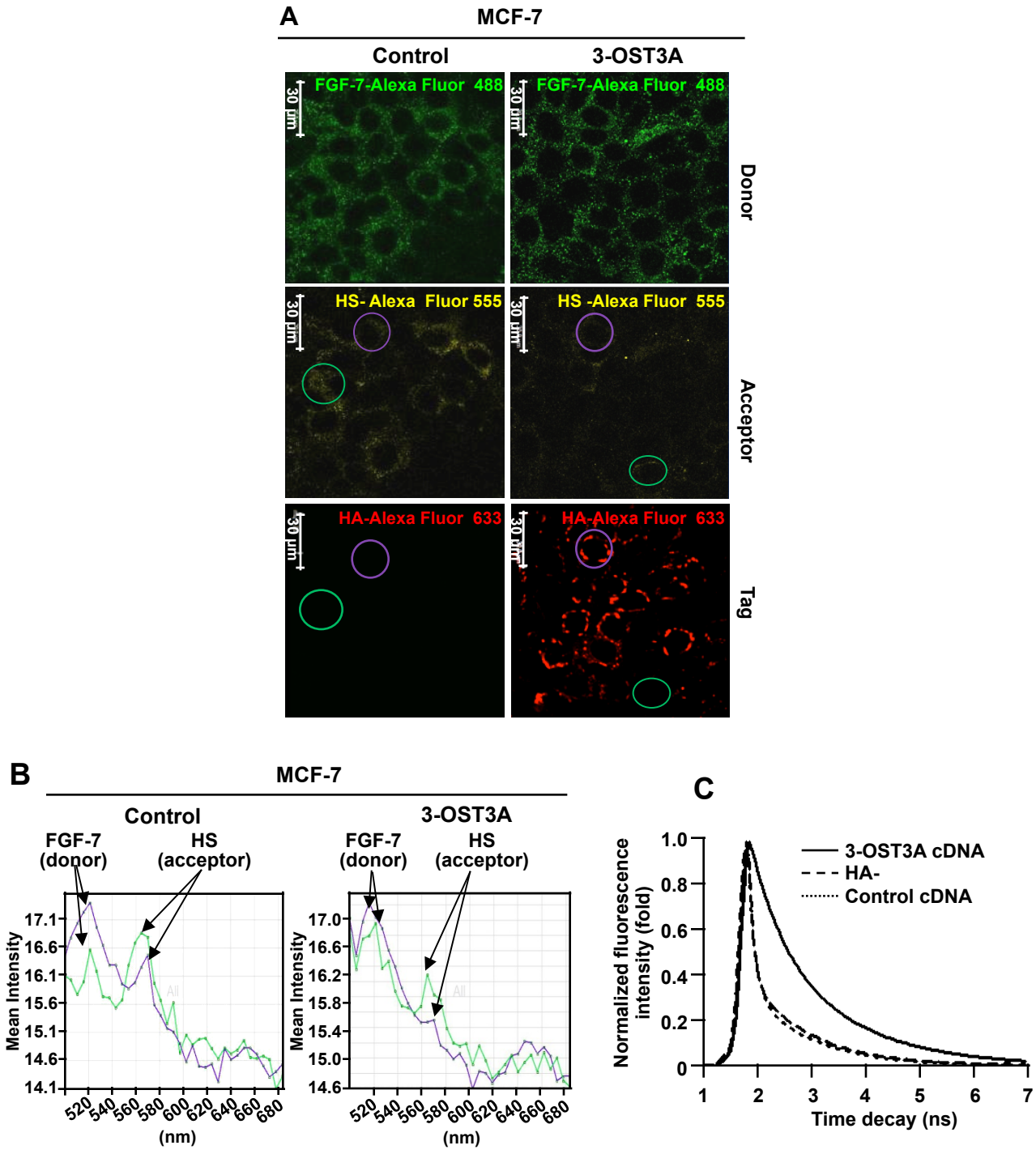

Figure S4. Restoration of 3-OST3A expression in MCF-7 cells inhibits FGF-7-HS interactions. **A**, Confocal microscopy analysis of FRET between FGF-7 and HS in empty vector (control) and 3-OST3A-HA cDNA stably transfected MCF-7 cells (3-OST3A). Upper panels show fluorescence signal of donor excited at 488 nm in the presence of acceptor. Middle panels show fluorescence signal of the acceptor produced by energy transfer from the donor. Lower panels show 3-OST3A-HA positive cells in red color detected by anti-HA and AlexaFluor 633 conjugated antibodies. Scale bar = 30 µm. **B**, Fluorescence spectra (lambda-scan) analysis from two regions of interest (green and purple circles in panel C of Figure S5A). Specifically, in 3-OST3A cDNA transfected cells, green and purple curves correspond to a HA negative (HA-) and a 3-OST3A-HA expressing (HA+) cell, respectively. **C,** lifetime decay experiments showing the changes of the lifetime average of the donor in 3-OST3A-transfected cells compared to HA-negative and empty vector transfected cells.

Figure S5

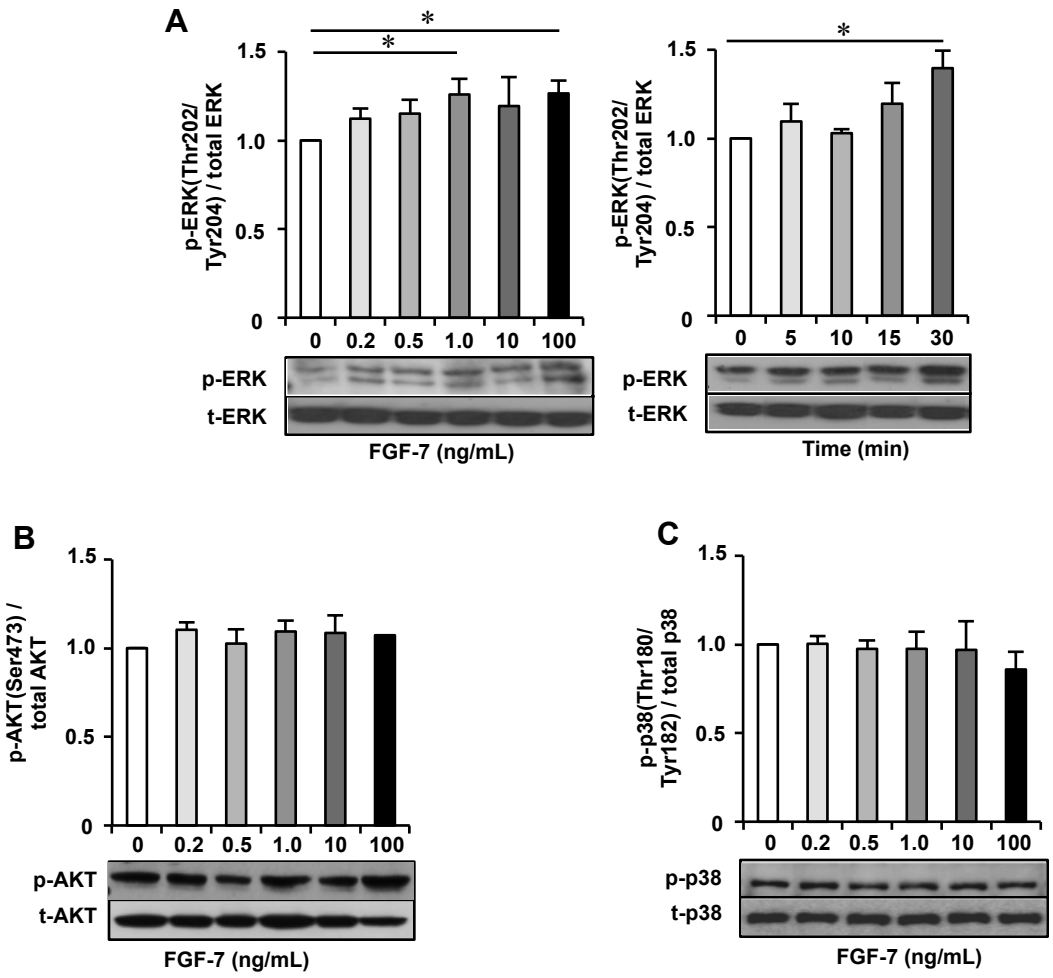

Figure S5. FGF-7-dependent signaling in MCF-7 cells. MCF-7 cells stably transfected with empty vector as control were serum-starved for 24 h and then stimulated with FGF-7 at the indicated concentrations. The lower panel shows a representative immunoblot analysis of cell lysates performed with **(A)**, anti-phospho-ERK1/2 (Thr202/Tyr204) and anti-ERK1/2, **(B)**, anti-phospho-AKT (Ser473) and anti-AKT. **(C)**, anti-phospho-p38 (Thr180/Tyr182) and anti-p38. The upper panel shows the relative intensity of immunoreactive bands of phosphorylated versus total protein, n=3. * $P < 0.05$

Figure S6

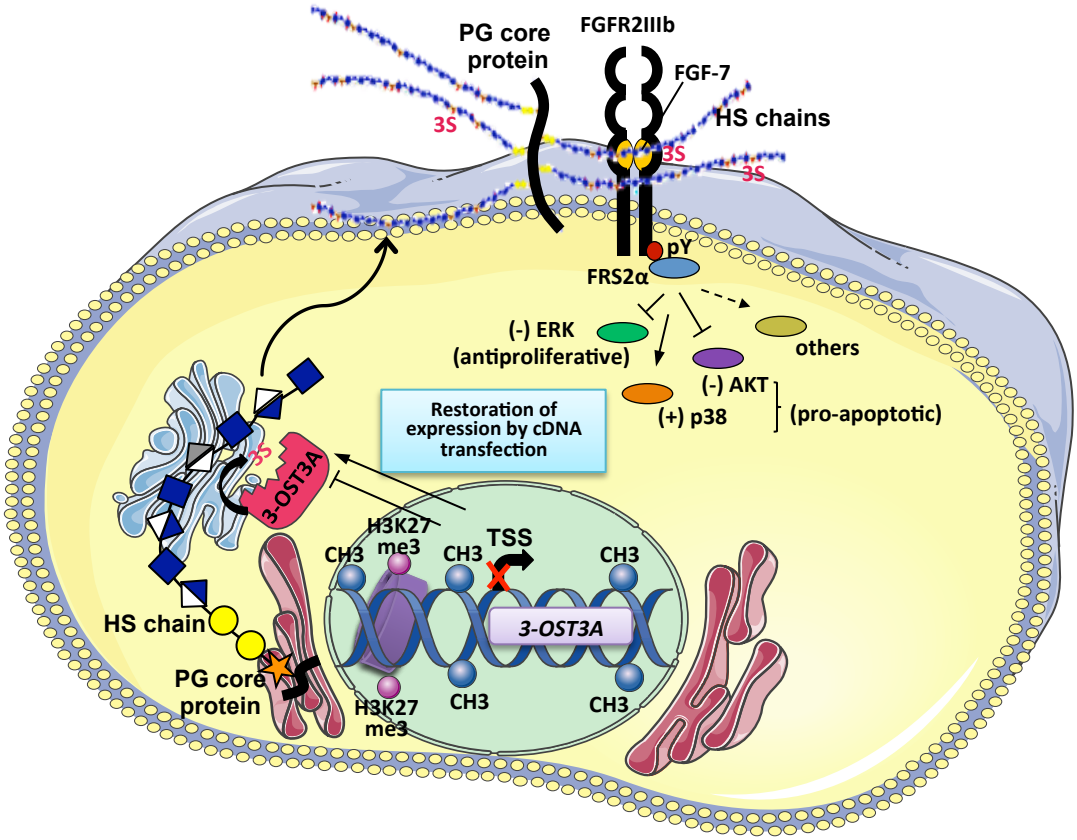

Figure S6. Schematic representation of the effect of 3-OST3A expression on HSPG-dependent FGF-7/FGFR2IIIb signaling axis. In MCF-7 cells, 3-OST3A gene expression is repressed upon DNA methylation and histone modifications such as H3K27me3. Upon cDNA transfection, restored expression results in modification of the interactions between FGF-7 and HS chains, leading to the modulation of downstream signaling pathway involving ERK, AKT and p38 that contribute to the anti-proliferative and pro-apoptotic properties of 3-OST3A in cancer cells.

Figure S7

A

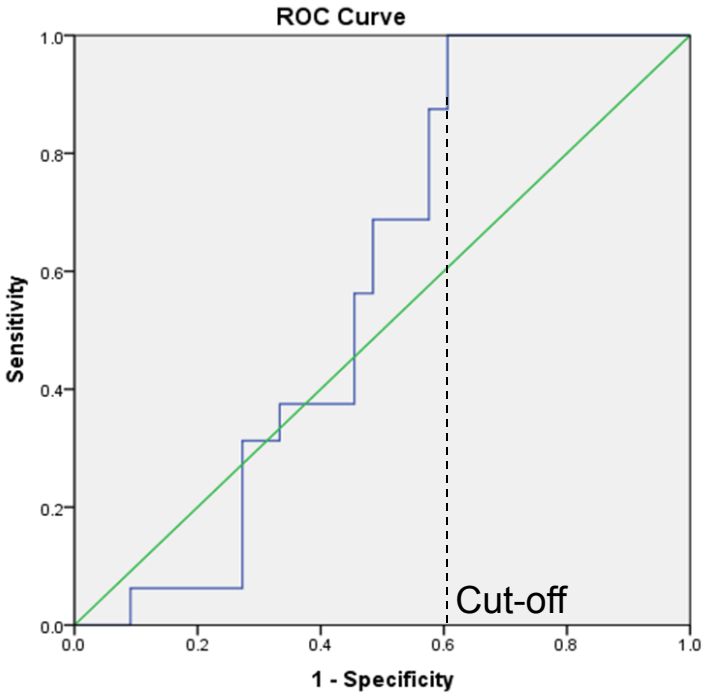

B

Coordinates of the Curve

Ratio 3-OST3A/TBP	Sensitivity	1 - Specificity	
.000000000000	1.000	1.000	
.015860238500	1.000	.970	
.021015433500	1.000	.939	
.029125074500	1.000	.909	
.041965004000	1.000	.879	
.059653177000	1.000	.848	
.080157168500	1.000	.818	
.093474592500	1.000	.788	
.097615924500	1.000	.758	
.102782652000	1.000	.727	
.108817730500	1.000	.697	
.115478558500	1.000	.667	
.119479650000	1.000	.636	
.122268318500	1.000	.606	Cut-off
.126126680500	.938	.606	
.133309235000	.875	.606	
.139679732000	.875	.576	
.141655389500	.813	.576	
.146349870500	.750	.576	
.151137535500	.688	.576	
.152955963000	.688	.545	
.156675436000	.688	.515	
.160600146500	.688	.485	
.167968313500	.625	.485	
.179929785000	.563	.485	
.185475404000	.563	.455	
.188277119500	.500	.455	
.194741757000	.438	.455	
.203910946500	.375	.455	
.210903022000	.375	.424	
.213456865000	.375	.394	
.221244076000	.375	.364	
.233433208000	.375	.333	
.242952986000	.313	.333	
.266251985500	.313	.303	
.286277597500	.313	.273	
.291418829000	.250	.273	
.300390024000	.188	.273	
.309285800000	.125	.273	
.313813280500	.063	.273	
.319874875000	.063	.242	
.327127306500	.063	.212	
.345561049000	.063	.182	
.384521402500	.063	.152	
.447172507500	.063	.121	
.488635170000	.063	.091	
.500546140000	.000	.091	
.548432914000	.000	.061	
.613344378000	.000	.030	
1.000000000000	.000	.000	

Figure S7. Association between 3-OST3A expression level and HER2+ breast cancer recurrence. **A**, Receiver Operating Characteristic (ROC) curve for cancer recurrence in HER2+ breast tumors in association with 3-OST3A level. The optimal cut-off was determined by Youden Index corresponding to the greatest vertical distance between ROC curve and the diagonal line. This index cut-off value that maximized the sum of sensitivity and specificity was determined for 3-OST3A expression level in HER2+ breast tumors. **B**, Tumors expressing a ratio of 3-OST3A/Tata Binding Protein (TBP) mRNA superior to 0.1222683 were defined as 3-OST3A positive, while tumors expressing a ratio of 3-OST3A/TBP mRNA ranging from 0 to 0.1222682 were defined as 3-OST3A negative.

Figure S8

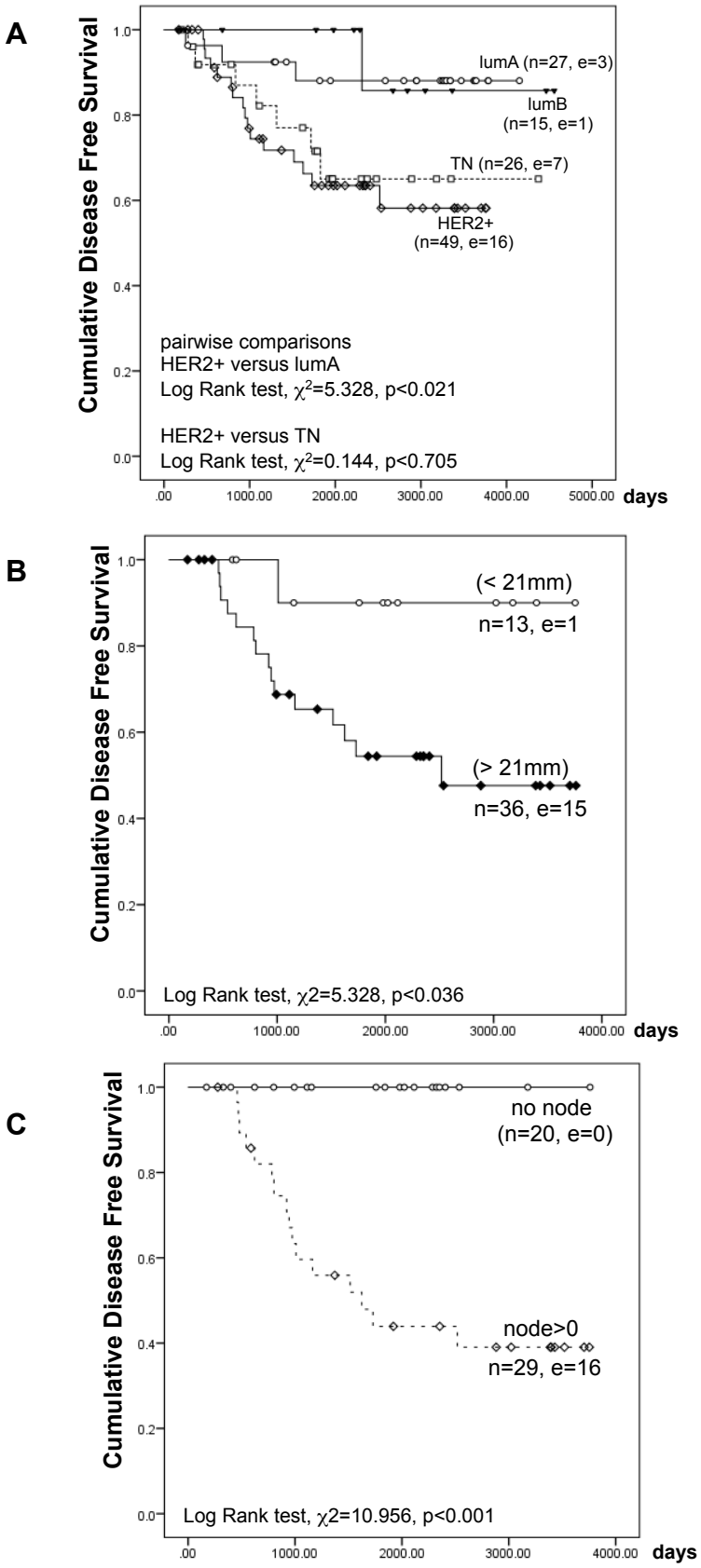

Figure S8. Kaplan-Meier survival curves of patients with breast cancer based on different pathological markers. **A**, Kaplan-Meier disease free survival curves of patients with breast cancer based on subtypes (luminal A, lumA; luminal B, lumB; triple negative, TN and HER2+). Number of breast tumors analysed, n=117. **B**, Kaplan-Meier disease free survival curves of HER2+ breast cancer patients correlated with tumor size. **C**, Kaplan-Meier disease free survival curves of HER2+ breast cancer patients correlated with presence of lymph node metastatis (invaded lymph node). Censored cases are shown on the curves. Log-rank analyses, *P* values, number of patients (n) and events (e) are indicated.

Supplementary Materials and Methods

Cell culture, drug treatment and gene transfection

SKBR3, MCF-7, BT-474, MDA-MB-231, MDA-MB-453 and MDA-MB-468 cells were maintained in Dulbecco's Modified Eagle Medium (DMEM) 4.5 g/L glucose supplemented with 10% (v/v) fetal bovine serum (FBS, Gibco), penicillin (1 U/mL)/streptomycin (1 µg/mL), L-glutamine (2 mM) and non-essential amino acids (NEAA, 0.1 mM). T-47D cells were cultured in RPMI-1640 Medium, supplemented with 10% (v/v) FBS, penicillin (1 U/mL)/streptomycin (1 µg/mL), L-glutamine (2 mM) and bovine insulin (0.2 U/mL). MCF-10A cells were maintained in DMEM-F12 medium, supplemented with 5% (v/v) donor horse serum, penicillin (1 U/mL)/streptomycin (1 µg/mL), 1% (v/v) L-glutamine (2 mM), epidermal growth factor (EGF, 20 ng/mL), insulin (10 µg/mL), cholera toxin (100 ng/mL) and hydrocortisone (0.5 µg/mL). All cell lines were grown at 37°C in a 5% CO_2 incubator under humidified atmosphere. MCF-7 and MDA-MB-231 cells were treated with 5-aza-2'-deoxycytidine (Aza, Sigma) at 2 and 4 µM concentration for 9 days, while controls were exposed to vehicle only (Phosphate Buffered Saline, PBS). During drug exposure, cells were passaged twice and medium containing Aza or vehicle was changed every 2 days. Trichostatin A (TSA, Sigma) at a concentration of 300 nM, or vehicle only (dimethylsulfoxide, DMSO) was added to cultures 24 h before the end of the experiment.

The plasmid pcDNA3.1(+)-3-OST3A-hemagglutinin (HA) or pcDNA3.1(+) was transiently or stably transfected into MCF-7, MDA-MB-231 and SKBR3 cells. All transient transfections were performed by electroporation following manufacturer's recommendations (Nucleofector™ Protocols, Lonza). For stable expression, the transfection protocol was optimized using pEGFP-N1 vector (Clontech). Briefly, 3×10^5 cells/well were seeded onto 6-well plates 24 h before transfection using 2 µg plasmid DNA and 15 µL Exgen 500 reagent (Euromedex) per well. Selection of stable transfectants was performed using 1.5 mg/mL geneticin (G418, Gibco). Resistant colonies were isolated and expression of 3-OST3A-HA recombinant protein in the individual colonies was verified by western blotting using anti-HA antibodies (Table S7). Two colonies stably expressing 3-OST3A (A and B) or stably transfected with pcDNA (A and B) were selected for xenograft experiments.

siRNAs against 3-OST3A were designed and synthesized by Eurogentec. Two 3-OST3A siRNAs (Table S8) and a negative control siRNA (Qiagen) were transfected in SKBR3 cells by electroporation following the manufacturer's recommendations (Nucleofector™ Protocols, Lonza). siRNA inhibition efficiency was verified by RT-qPCR analysis of 3-OST3A mRNA level (>80%) using primers listed in Table S9, and by immunodetection of the recombinant 3-OST3A-HA protein using anti-HA antibodies.

RT-qPCR analysis

Purified RNA extracted from cultured cells was reverse-transcribed to cDNA using the SuperScript® VILO™ cDNA synthesis kit (Invitrogen). qPCR reactions were performed using SYBR Green I (Qiagen) in a LightCycler® system (Roche). Specificity of the amplification was verified using melting curve analysis. The $2\text{-}\Delta\Delta C_t$ method was used to determine relative gene transcript levels normalized to *RP29* reference gene. The primers used

are listed in Table S9. Conditions for the qPCR reaction were 94°C for 15 min followed by 40 cycles at 94°C for 15 s, 55°C (*RP29*) or 60°C (*3-OST3A*) for 1 min, and ending with a final step of 15 s at 94°C, 1 min at 60°C and 15 s at 94°C corresponding to melt curve stage.
For tumor analysis, approximately 10 mg of tissue (> 40% of tumor cells) was homogenized in 75 µL of QIAzol lysis reagent (Qiagen) and total RNA was extracted as described above (Qiagen). RNA quality was assessed using the BioAnalyzer 2100™ (Agilent Technologies) prior to RT-qPCR analysis and all samples with a ratio of 28S/18S < 1.2 were discarded. Reverse transcription was performed with 0.5 µg of total RNA, using the cloned AMV Reverse Transcription kit (Invitrogen) and cDNA quality was confirmed by PCR amplification of actin. Samples for which actin mRNA could not be amplified after 30 cycles of PCR were discarded. PCR conditions were as above.

CpG island identification and methylation status analysis

Genomic DNA (gDNA) extracted from MCF-10A, SKBR3, MCF-7, BT-474, T-47D, MDA-MB-231, MDA-MB-453 and MDA-MB-468 cells was submitted to bisulfite conversion using the EpiTect Bisulfite kit (Qiagen) according to the manufacturer's instructions. Converted gDNA was used for amplification of two regions of interest by nested-PCR using sense and antisense primers listed in Table S10. Conditions for the first PCR reaction were 94°C for 8 min followed by 20 cycles at 94°C for 30 s, 55°C for 30 s, 72°C for 30 s, ending with a final extension step of 10 min at 72°C. For the second round of PCR, conditions were 94°C for 8 min followed by 35 cycles at 94°C for 30 s, 60°C for 30 s, 72°C for 30 s, and finally 10 min at 72°C. PCR products were purified and subcloned using the TOPO TA® Cloning kit (Invitrogen) and transformed into One Shot® TOP10 competent cells (Invitrogen). Plasmid DNA of at least three individual clones was sequenced to identify uncovered cytosines within CpG dinucleotides, which correspond to methylated sites.

Chromatin immunoprecipitation (ChIP) assay

For the ChIP assay, 1×10^6 cultured cells were harvested and fixed with 1% (w/v) *para*formaldehyde for 10 min at room temperature with gently stirring. Glycine buffer (1.25 M) was added into the mix to stop the cross-linking reaction. The cell pellet was collected and sonicated to shear chromatin DNA to an average length of 500 bp-fragments. The input DNA was quantified by spectrofluorimetry on a Qubit (Invitrogen) apparatus using Quant-iT dsDNA HS Assay kit (Invitrogen). Protein G-coated magnetic beads were incubated with primary antibodies (listed in Table S11) at 4°C for at least 2 h, prior to incubation with chromatin DNA at 4°C overnight. Crosslinking was reversed by overnight incubation at 65°C, and ChIP DNA product was purified and isolated using the IPure kit (Diagenode) for subsequent PCR reaction. The PCR primers (Table S12) were designed by Premier Primer 5.0 software to amplify 3 adjacent regions, -347/-129, +216/+393 and +468/+605 to the TSS of human *3-OST3A* gene.

Protein extraction and western blotting

Cells cultured in 6-well plates were harvested and lysed in 100 µL of NP-40 lysis buffer containing 1% (v/v) NP-40, 20 mM Tris-HCl (pH 8.0), 137 mM NaCl, 10% glycerol, 2 mM

EDTA supplemented with protease and phosphatase inhibitor mixture (Roche). Protein concentration was determined by using a Bradford protein assay kit (Biorad). Lysates containing 20 μg of protein were subjected to sodium dodecyl sulfate (SDS)-PAGE on 10% (w/v) polyacrylamide gels. Proteins were transferred onto Immobilon-P® polyvinylidene (PVDF) membrane (Millipore) and incubated in the presence of primary antibodies listed in Table S7. Following incubation with anti-mouse or anti-rabbit peroxidase conjugated secondary antibodies (Cell Signal Technology), proteins were visualized by the Enhance Chemiluminescence (ECL) western blot detection kit (Santa Cruz).

Cell proliferation assay

Cells transfected with 3-OST3A-HA cDNA or with siRNA 3-OST3A and corresponding controls were seeded onto 24-well plates at a density of 2×10^4 cells per well for MCF-7 and MDA-MB-231 cells and 4×10^4 cells per well for SKBR3 cells. Twenty-four hours after transfection, cells were harvested each day during a 4-day period by scraping in 50 μL lysis buffer (1% (w/v) SDS-PBS). Cell proliferation was evaluated by measuring the DNA content in each sample by spectrofluorimetry using the Quant-iT dsDNA HS Assay kit (Invitrogen). The proliferation assay was also performed on SKBR3 cells treated with 0, 20 and 40 μg/mL of trastuzumab 24 h after transfection.

Annexin V flow cytometry cell apoptosis assays

Cells transfected with 3-OST3A-HA cDNA, and with siRNA 3-OST3A and corresponding controls were seeded onto 6-well plates at a density of 1.5×10^5 cells per well. 48 h following transfection, cells were detached by cell dissociation enzyme-free PBS-based buffer (Gibco), washed 3-times in PBS, and stained with AlexaFluor 488-conjugated annexin V and propidium iodide (PI) dyes (Invitrogen). The externalization of phosphatidylserine (PS) and the permeability to PI were evaluated by flow cytometry by collecting data from 10,000 events per sample.

TUNEL imaging assay

MCF-7 cells were transfected with empty vector (control) or with 3-OST3A-HA cDNA by electroporation and seeded onto Lab-Tek chambers at a density of 2×10^4 cells per well. Forty-eight hours after transfection, cells were prepared to TUNEL (terminal deoxynucleotidyl transferase-dUTP nick and labeling) assay following the manufacturer's recommendations (Click-iT® TUNEL AlexaFluor® Imaging Assay, Invitrogen) to detect fragmented DNA. Cells were washed with PBS and fixed in 4% (w/v) *para*formaldehyde at RT for 15 min and permeabilized with 0.25% (w/v) Triton-X 100 in PBS at RT for 20 min, washed 2-times with deonized water before to proceed to TdT (terminal deoxynucleotidyl transferase) reaction. Cells were incubated with TdT reaction buffer at RT for 10 min and then with TdT reaction cocktail containing TdT reaction buffer, EdUTP and TdT for 60 min at 37°C. Cells were washed 2-times with 3% (w/v) BSA-PBS for 2 min before to proceed to Click-iT reaction. Cells were incubated with Click-iT reaction cocktail containing the Click-iT reaction buffer (which contains AlexaFluor 594 azide) and the Click-iT® reaction buffer additive at RT for 30 min protected from light, washed with 3% (w/v) BSA-PBS for 5 min. In parallel, a

positive control was performed using DNase I which generates strand breaks in the DNA. Images were analyzed by confocal laser scanning microscopy on a Leica TCS SP5-X-AOBS apparatus.

In vivo mouse xenograft tumor model

The animal protocol was approved by the regional Ethical Committee (Institut Pasteur, Lille, France). Engineered MCF-7 cell lines stably transfected with 3-OST3A-HA or pcDNA vector were inoculated subcutaneously into 6-week-old female SCID mice. 5×10^6 cells were injected into each mouse, and four mice were used by group for each individual experiment. The tumor size was assessed once per week using external measurement of the two largest orthogonally diameters using a Vernier caliper. Tumor volume was calculated using the formula $V = a*b^2/2$ where "a" is the largest measured diameter and "b" the shortest. For ethical considerations, animals were euthanized when the tumor diameters exceeded 1 cm and had about 1 g of tumor weight (*i.e.* 5% of animal weight). The protocol was repeated twice using two independent 3-OST3A- and control pcDNA-engineered cell lines.

Confocal microscopy observation of FGF-7 cell-surface binding

Cells cultured in Lab-Tek chambers (Thermo-scientific) were serum-starved for 24 h, incubated with freshly prepared medium containing recombinant human FGF-7 (R&D system, 0.5 ng/mL) for 30 min or containing same volume of PBS, rinsed 3-times and fixed in 4% (w/v) *para*formaldehyde at room temperature (RT) for 10 min. After blocking with 5% (w/v) bovine serum albumin (BSA)-PBS, cells were incubated with anti-HS antibody (10E4 epitope, Seikagaku Corp.) in 1% (w/v) BSA-PBS at RT for 45 min, washed 3-times with PBS, incubated with AlexaFluor 555-conjugated donkey anti-mouse antibodies (Invitrogen) for 45 min, and finally washed with PBS. For FGF-7 visualization, cells were incubated with goat anti-human FGF-7 (Santa Cruz) and then AlexaFluor 488-conjugated rabbit anti-goat antibodies (Invitrogen). For nucleus staining, cells were permeabilized with a 0.2% (w/v) BSA-PBS solution containing 0.1% (w/v) Triton-X 100 at RT for 10 min, washed 3 times with PBS, incubated with TOPRO®-3 Iodide (642/661) (Invitrogen) in PBS for 10 min, and washed 3 times with PBS before observation. Images were analyzed by confocal laser scanning microscopy on a Leica TCS SP5-X-AOBS apparatus. All primary and secondary antibodies are listed in Table S7.

FLIM-based FRET assay of FGF-7-HS interactions

A Leica TCS SP5-X-AOBS microscope equipped with an acousto-optical beamsplitter and WLL lasers was used with a ×40/0.8 water immersion objective for image captures and spectra measurements. In all cases, excitation wavelength was 488 nm for FRET donor and adjusted to minimize the excitation of the acceptor (AlexaFluor 555). Fluorescence lifetime measurements were performed with a time-correlated single photon counting technique using a WLL laser with a pulse width from 120 fs and a repetition rate of 76 MHz. For lifetime imaging in FLIM assay, a SPC-730 TCSPC imaging module (Becker&Hickl, Berlin) was interfaced (signals, Pixel Clock, Frame Sync) to the scan controller of the Leica TCS SP5-X-AOBS laser scanning microscope. Temporal histogram depicting the AlexaFluor 488

fluorescence lifetime distribution was obtained by a biexponential fit of the fluorescence decay and the decay analysis evaluated by time-correlated single photon counting was performed using the SPCImage software (Becker&Hickl GmbH).

Flow cytometry analysis of FGF-7 cell-surface binding

Cells cultured in 6-well plates were treated with FGF-7 as above. Then, 3×10^5 cells per assay were incubated with 3 μg goat anti-human FGF-7 antibodies in 100 μL 0.5% BSA-PBS at 4°C for 15 min, washed once with PBS, incubated with AlexaFluor 488-conjugated rabbit anti-goat antibodies (Invitrogen) for 15 min, and finally washed once with PBS. Cells samples were fixed in 4% (w/v) *para*formaldehyde and analyzed on a flow cytometer (Gallios, Beckman Coulter). Data from 10,000 events per sample were collected and staining was normalized to the control cells (stained with secondary antibodies only).

Clinical samples and tumor grade, estrogen receptor, progesterone receptor and HER2 status analysis

Previously untreated operable primary breast tumors from 117 Caucasian women (age range 32-89 years, median age 60 years) with sufficient tumor tissue surplus to diagnostic requirements and complete clinical and pathological data, were analyzed (Table S2). Tumor tissues were macro-dissected by a specialist breast pathologist and snap frozen in liquid nitrogen prior to storage at -80ºC.

Immunohistochemical staining was carried out on 4 μm sections of formalin-fixed paraffin embedded tumors with the mouse monoclonal anti-estrogen receptor alpha (ER) antibody 6F11 (Novocastra Laboratories Ltd), progesterone receptor (PR) antibody clone 16, (Novocastra Laboratories Ltd) and mouse monoclonal anti-HER2 antibody CB11 (Novocastra Laboratories Ltd). Additional analyses were performed according to histological tumor grade and tumor size evaluated by a specialist consultant breast pathologist. ER status (as ER negative 0-3 versus ER positive 4-18) was determined by the "quickscore" method. Briefly, immuno-reactivity scored semi-quantitatively for both the intensity and the proportion of cells staining: intensity was given scores 0-3 (no staining = 0, light staining = 1, moderate staining = 2, strong staining =3) and proportion was given scores 1-6 (0-4% = 1, 5-20%= 2, 21-40% = 3, 41-60% = 4, 61-80% = 5, 81-100% = 6). The two scores were then multiplied to obtain the final result of 0 - 18.

Statistical analysis

Data obtained by clinical studies were subjected to following statistical analysis. The difference of 3-OST3A expression level between breast cancer subtypes was evaluated by Kruskal-Wallis test (null hypothesis rejected) followed by Mann-Whitney test for pairwise comparison. Breast cancer-related survival (abbreviated to overall survival) and breast cancer disease free survival (abbreviated to disease free survival or cancer recurrence) were followed and non-breast cancer deaths were censored at the time of death. Statistical analysis was performed using SPSS software (SPSS version 21.0) for Chi-squared, 2-sided Fisher's Exact Test and Kaplan-Meier analyses. These univariate analyses do test for association between variables in a pair-wise manner (*e.g.* A *versus* B), but without adjusting for influence exerted

by other associated variables (*e.g.* both A and B may be associated with confounding variables C, D, E…). To adjust for possible confounding variables, the selected variables were interrogated by the multivariate methods of Cox's proportional hazards regression model (CR) with associated Hazard Ratios (HR), both utilizing the backwards step-wise elimination method. The results of the univariate and multivariate analyses were consistent, and for clarity and brevity only the results of CR and Kaplan-Meier analyses are presented. Throughout the analyses, the null hypothesis was rejected at a α level of 10% ($P < 0.10$), and observations considered to be marginal (*i.e.* unworthy of further analysis) for an α level between 5% and 10% ($0.05 \leq P < 0.10$) and significant at 5% ($P < 0.05$). The P value represents the probability of error that is involved in accepting our observed result as valid. For example, $P = 0.05$ indicates a 5% probability for the relation between the variables occurring by chance.

Supplementary Tables

Table S1. Classification of breast cancer cell lines

Cell line	Classification	Immunoprofile
MCF-7	Luminal A	ER^{+}, $PR^{+/-}$, $HER2^{-}$
T-47D	Luminal A	ER^{+}, $PR^{+/-}$, $HER2^{-}$
BT-474	Luminal B	ER^{+}, $PR^{+/-}$, $HER2^{+}$
MDA-MB-468	TN	ER^{-}, PR^{-}, $HER2^{-}$
MDA-MB-231	TN	ER^{-}, PR^{-}, $HER2^{-}$
SKBR3	HER2+	ER^{-}, PR^{-}, $HER2^{+}$
MDA-MB-453	HER2+	ER^{-}, PR^{-}, $HER2^{+}$

ER, estrogen receptor; HER2+, human epidermal growth factor receptor 2; PR, progesterone receptor, TN, triple negative

Table S2. Description of the characteristics of the breast cancer patients

Variables		Number of patients
primary breast tumors		117
median age follow up		61.5 (range 28.7-89.1 years) 6.85 (0.29-13.7 years)
Grade	1 2 3	2 24 91
type	ductal others	96 21
clinico-pathological subtype	TN LumA LumB HER2+	26 27 15 49
size	<21mm ≥21mm	24 93
Invaded lymph nodes (node > 0)	none presence	53 64
patient outcome	disease free recurrence alive death	90 27 99 18
3-OST3A	ratio to TBP mRNA	0.191 (0.0021-0.8842)
3-OST3A cut-off (0.12)	0 1	48 69

TBP, Tata Binding Protein

Table S3. Univariate analysis of association between 3-OST3A expression and cancer recurrence

		Recurrence		
		-	+	Total
3-OST3A	**-**	13	0	13
	+	20	16	36
Total		33	16	49

Results are expressed as number of patients, Fisher's *t* test, $P < 0.004$

Table S4. Univariate analysis of association between tumor size and presence of lymph node

		Invaded Lymph node		
		none	presence	Total
size	**< 21 mm**	8	5	13
	≥ 21mm	12	24	36
Total		20	29	49

Results are expressed as number of patients, Fisher's *t* test, $P < 0.104$

Table S5. Univariate analysis of association between 3-OST3A expression and presence of lymph node

		Invaded Lymph node		
		none	presence	Total
3-OST3A	**-**	8	5	13
	+	12	24	36
Total		20	29	49

Results are expressed as number of patients, Fisher's *t* test, $P < 0.104$

Table S6. Univariate analysis of association between tumor size and 3-OST3A expression

		Size		
		< 21 mm	≥ 21mm	Total
3-OST3A	**-**	5	8	13
	+	8	28	36
Total		13	36	49

Results are expressed as number of patients, Fisher's *t* test, $P < 0.288$

Table S7. Antibodies and conditions used for immunoblotting and immunofluorescence experiments

Antibody	Provider	Source	Dilution
Human phospho-FGFR1-4 (Y653/Y654)	R&D systems	rabbit	1:1000
Bek (C-17) or FGFR2	Santa Cruz Biotechnology	rabbit	1:200
Phospho-FRS2-α (Tyr196)	Cell Signaling Technology	rabbit	1 :1000
FRS2	Santa Cruz Biotechnology	rabbit	1 :200
Phospho-AKT (Ser473)	Cell Signaling Technology	rabbit	1:1000
AKT	Cell Signaling Technology	rabbit	1:1000
Phospho-p38 MAPK (Thr180/Tyr182) (D3F9)	Cell Signaling Technology	rabbit	1:1000
p38 MAPK	Cell Signaling Technology	rabbit	1:1000
Phospho-p44/42 MAPK (ERK1/2) (Thr202/Tyr204) (D13.14.4E)	Cell Signaling Technology	rabbit	1:1000
P44/42 MAPK (137F5)	Cell Signaling Technology	rabbit	1:1000
Poly ADP-ribose polymerase (PARP)	Cell Signaling Technology	rabbit	1:1000
Cleaved PARP (Asp214)	Cell Signaling Technology	rabbit	1:1000
Bax (N-20)	Santa Cruz Biotechnology	rabbit	1:500
Bcl-2 (C-2)	Santa Cruz Biotechnology	mouse	1:200
Cleaved caspase 9 (Asp315)	Cell Signaling Technology	rabbit	1:1000
Anti-HA	Sigma-Aldrich	rabbit	1:10,000
β-actin	Sigma-Aldrich	mouse	1:3000
FGF-7 (S-20)	Santa Cruz Biotechnology	goat	1:50
HS (10E4 epitope)	Seikagaku Corporation	mouse	1:50
GM130	BD Transduction Laboratories	mouse	1:200
Anti-mouse IgG, HRP-linked antibody	Cell Signalling Technology	horse	1:2000
Anti-rabbit IgG, HRP-linked antibody	Cell Signaling Technology	goat	1:2000
Anti-rabbit IgG (whole molecule)-alkaline phosphatase antibody	Sigma-Aldrich	rabbit	1:10,000
AlexaFluor®488 rabbit anti-goat	Invitrogen Life Technologies	rabbit	1:200
AlexaFluor® 555 donkey anti-mouse	Invitrogen Life Technologies	donkey	1:200
AlexaFluor® 633 goat anti-rabbit	Invitrogen Life Technologies	goat	1:500

Table S8. Synthetic siRNA sequences used for RNA interference experiments

Gene	RefSeq		Sequence	Size (bp)	Position	Efficiency	
						RNA (%)	Protein
3-OST3A	NM_006042.1	Target 1	5′-CGTCCCTTTACGTCTTCTA-3′	19	899-917		
		Sense 1	5′-CGUCCCUUUACGUCUUCUA-3′			88.3 ± 6.3	ND
		Antisense 1	5′-UAGAAGACGUAAAGGGACG-3′				
		Target 2	5′-ATCTGGTAGAACTTGAGGT-3′	19	1970-1988		
		Sense 2	5′-ACCUCAAGUUCUACCAGAU-3′			71.7 ± 4.9	ND
		Antisense 2	5′-AUCUGGUAGAACUUGAGGU-3′				

Experiments were performed using two sets of siRNA (1 and 2). Efficiency of siRNA inhibition was evaluated using MCF-7 stably transfected with 3-OST3A cDNA. mRNA level was evaluated by RT-qPCR (mean ± SEM, n=3) and protein expression by immunoblotting using anti-HA antibodies, ND, not detectable (n=3).

Table S9. Sequence of primers used for RT-qPCR analysis

Gene		Primers	Size (bp)	Tm (°C)
3-OST3A	Sense	5'-CAGTGCCCTCTCCACCTC-3'	108	60
	Antisense	5'-GCCAGGCAGTAGAAGACGTAA-3'		

Table S10. Sequence of primers used for nested-PCR amplification

Gene		Primers	Localisation to TSS	Size (bp)	Number of CpG
3-OST3A 5′ Region	Out sense	5′-TAGTGTTAAGAGGGGAGTAG-3'	-454 to +281	735	46
	Out antisense	5′-CTTTCTCTAATCCCCTTACC-3′			
	In sense	5′-ATTAAGTTAGTGGCGTTTGGG-3′	-360 to +120	480	
	In antisense	5′-CTACTCTTAAACCCCACCTAT-3′			
3-OST3A 3′ Region	Out sense	5′-ATAGGTGGGGTTTAAGAGTAG-3′	+100 to +768	668	54
	Out antisense	5′-CCGACCATACTAAACCTAAAC-3′			
	In sense	5′-GGAAAGGGGATTAGAGAAAG-3′	+262 to +746	484	
	In antisense	5′-CCGACAAATACCAAAACATCC-3′			

First round of PCR was performed with primers “Out sense” and “Out antisense” and second round of PCR was performed with primers “In sense” and “In antisense”. TSS, transcription start site.

Table S11. Antibodies used for ChIP analyses.

Antibody	Catalog information	Source	Quantity /ChIP
DNMT1 (mAb)	Active Motif 39204	mouse	5-10 µg
DNMT3A (mAb)	Active Motif 39206	mouse	5-10 µg
DNMT3B (mAb)	Active Motif 39207	mouse	5-10 µg
Histone H3K4me3 (pAb)	Active Motif 39915	rabbit	5-10 µg
Histone H3K9me3 (pAb)	Active Motif 39161	rabbit	5-10 µg
Histone H3K27me3 (pAb)	Active Motif 39155	rabbit	5-10 µg
EZH2 (mAb)	Active Motif 39875	mouse	1-3 µg
SUZ12 (pAb)	Diagenode C15310029	rabbit	5 µg
HDAC1 (pAb)	Invitrogen Life technologies 49-1025	rabbit	5-10 µg
MeCP2 (pAb)	Diagenode pAb-052-050	rabbit	5-10 µg
Sin3A (pAb)	Active Motif 39865	rabbit	5-10 µg

Monoclonal (m), polyclonal (p) antibodies (Ab).

Table S12. Sequence, size, location relative to TSS and Tm of PCR primers for ChIP analyses

		Primers	Size (bp)	Location to TSS	Tm (°C)
Set 1	Sense	5′-GCGTCTTGGGTGGAAGTCAG-3′	219	-347/-129	65
	Antisense	5′-TGGGATGGAGAAAAGGTGGC-3′			
Set 2	Sense	5′-CCTTGGCTGAGAGAACCTGAAC-3′	178	+216/+393	65
	Antisense	5′-TCAGCGATCCTGCATCACTGGC-3′			
Set 3	Sense	5′-GCCAAGGCTGCCCCAAGCTCA-3′	138	+468/+605	65
	Antisense	5′-CAGGATCCCTGCCTCCAGTC-3′			